TECHNISCHE UNIVERSITÄT WIEN

GEO

DIPLOMARBEIT

Characterization of lake beds with the transient electromagnetic method

zur Erlangung des akademischen Grades

Diplom-Ingenieur

im Rahmen des Studiums

Geodäsie und Geoinformation

eingereicht von

Philipp Högenauer BSc.

Matrikelnummer: 01425018

ausgeführt im Forschungbereich Geophysik (E120.3)
am Department für Geodäsie und Geoinformation
der Fakultät für Mathematik und Geoinformation der Technischen Universität Wien

Betreuung
Associate Prof. Dr.rer.nat. Adrian Flores-Orozco
Univ.Ass. Dipl.-Ing. Lukas Aigner

Wien, im Dezember 2020

(Unterschrift Verfasser) (Unterschrift Betreuer)

Eidesstattliche Erklärung

Ich nehme zur Kenntnis, dass ich zur Drucklegung meiner Arbeit unter der Bezeichnung

Diplomarbeit

nur mit Bewilligung der Prüfungskommission berechtigt bin.

Ich erkläre an Eides statt, dass ich die vorliegende Arbeit nach den anerkannten Grundsätzen für wissenschaftliche Abhandlungen selbstständig erstellt habe. Alle verwendeten Hilfsmittel, insbesondere die zugrunde gelegte Literatur, sind in dieser Arbeit genannt und aufgelistet.

Das Thema dieser Arbeit wurde von mir bisher weder im In- noch Ausland einer Beurteilerin/einem Beurteiler zur Begutachtung in irgendeiner Form als Prüfungsarbeit vorgelegt. Diese Arbeit stimmt mit der von den Begutachterinnen/Begutachtern beurteilten Arbeit überein.

Wien, im Dezember 2020

Philipp Högenauer

Danksagung

Zu Beginn möchte ich mich bei meinem Betreuer, Adrian Flores-Orozco bedanken, der mir die Möglichkeit gegeben hat, mich mit dem Thema Geophysik sehr ausführlich auseinanderzusetzen. Dadurch habe ich meine Leidenschaft für diese Thematik gefunden. Außerdem möchte ich mich für die kompetente Betreuung, die interessanten Diskussionen und die Hilfe bei verschiedensten Problemen bedanken.

Weiters möchte ich mich bei Lukas Aigner bedanken, für die Einführung und die Hilfe bei den Messungen, für die Hilfe bei dem ein oder anderen Programmier-Problem und für den generellen Beistand, wenn etwas nicht so funktioniert hat wie es sollte.

Bei Walter Loderer möchte ich mich bedanken für die technische Expertise, die mir von der Planung bis zum Bau des 'Schwimmrings' sehr geholfen hat.

Vor allem möchte ich mich aber bei meinen Eltern bedanken, die mir das Studieren und Wohnen in Wien ermöglich haben. Danke - mir ist bewusst, dass das nicht selbstverständlich ist! Danke, dass ihr immer an mich geglaubt habt und verständnissvoll wart.

Danke auch an Annika, für die (fast) kostenlosen Korrekturen.

Danke an meine 4 besten Freunde, für die gemeinsamen Abende, für die Gesprächsrunden und für die offenen Ohren, wenn ich Dampf ablassen musste. Danke fürs da sein, wenn ich euch brauche.

Danke auch an meine Kommilitonen, für die Ablenkungen in der Mittagspause, die Zeit die für das ein oder andere Bier draufging und die guten Erfahrungen die wir während des Studiums machen durften.

Zuguterletzt, danke El(l)i, für deine Fähigkeit mich immer wieder zu motivieren, mir andere Sichtweisen / Herangehensweisen zu zeigen, mich aufzubauen, wenn ich kein Licht am Ende des Tunnels mehr gesehen habe und für die Ablenkung, wenn mir alles zu viel wurde.

Kurzfassung

Im Zuge dieser Arbeit wurden transiente elektromagnetische (TEM) Messungen auf Seen durchgeführt. Ziel dieser Messungen war es, die Form des Grundes von Gewässern sowie den spezifischen elektrischen Widerstand des Wassers und der darunterliegenden geologischen Schichten zu bestimmen.

Für die Anwendung von TEM auf Wasser wurde ein schwimmfähiger Ring nach dem Vorbild von Matthias Bücker et al. (2020) gebaut. An diesem Ring wurde das Kabel für die TEM Antenne angebracht und diese wurde mit einem motorisiertes Boot über das Wasser gezogen.

Ein weiteres verwendetes Instrument war eine CTD (conductivity temperature depth)-Sonde. Mit ihrer Hilfe wurde die elektrische Leitfähigkeit des Wassers in-situ bestimmt. Anhand dieser Daten konnten in der Auswertung genauere Startmodelle angefertigt und Inversionen mit von vornherein bekannten Daten durchgeführt werden.

Zur Validierung der Ergebnisse wurde außerdem noch die elektrische Widerstandstomografie (kurz ERT) verwendet. Bei dieser Methode wird ein Kabel, an dem Elektroden angebracht sind, ebenfalls mit einem motorisiertem Boot hinterhergezogen. Die gemessene Größe ist hierbei ebenfalls der spezifische elektrische Widerstand.

Durch die verwendeten Methoden soll das Verständnis der Interaktion zwischen dem Grundwasser und dem Seewasser verbessert werden. Weiters können hydrogeologische Systeme mithilfe der genannten Verfahren auf Auswirkungen des Klimawandels untersucht werden.

Die Ergebnisse aus drei Fallstudien zeigen, dass es möglich ist mit TEM die Sedimentschicht von Seen zu bestimmen. Um Probleme zu vermeiden, sollte das verwendete Boot nicht aus Metall gebaut sein und bei den ERT Messungen sollte man sich vor dem Start jeder Messung vergewissern, dass das Kabel eine Linie bildet. Um die TEM Resultate verifizieren zu können, sind Zusatzinformationen sehr nützlich. Deswegen werden multi-methodische Ansätze empfohlen.

Abstract

In the course of this thesis, transient electromagnetic (TEM) measurements were carried out on lakes. The aim of these measurements was to determine the geometry of the water bottom and the electrical resistivity of the water and the underlying geological layers.
A buoyant ring was built according to the model of Matthias Bücker et al. (2020) for the application of TEM on the surface of the lakes. The cable for the TEM antenna was attached to this ring and the antenna was pulled over the water by a motorised boat where the measuring device was located.
Another instrument used was a CTD (conductivity temperature depth)-probe. It was used to determine the electrical conductivity of the water in-situ. Based on the CTD data, accurate start models could be created and inversions with a-priori information could be performed.
Electrical resistivity tomography (ERT) was also used to validate the results. For the collection of ERT, a cable with electrodes attached to the measuring device was pulled by a motorised boat. The measured value with ERT is the distribution of the electrical resistivity, resolved through the inversion of the field data.
The methods used aimed at improving our understanding of the interaction between surface- and groundwater, as well as the geological settings of the lakes. In addition, hydrogeological systems can be examined for the effects of climate change using the methods mentioned above.
The results from three case studies show that it is possible to determine the sedimentary layer underneath lakes with TEM. To avoid problems, a non-metal boat should be used. For ERT measurements it is important to make sure that the cable forms a line before starting each measurement. For verification of the TEM results, additional information is very useful. Therefore multi-methodical approaches are recommended.

Contents

List of Figures

List of Tables

1 Introduction

1.1 Motivation

The transient electromagnetic method - TEM (also called time domain electromagnetic method - TDEM) has originally been used for mineral exploration. Nowadays, two of the main fields for the application of TEM are general geological mapping and hydro-geological applications. Furthermore, the close relationship between the electrical conductivity that is measured by TEM, and hydrogeological properties such as porosity, clay content and saturation plays an important role (Goldman and Neubauer (1994)). A relatively new application for TEM is its usage on rivers, lakes and at sea. The application of waterborne TEM requires a floating construction where the cable is attached to conduct off-shore measurements. According to Butler (2009), research questions for waterborne TEM applications often relate to freshwater discharge pathways into the ocean, saline water intrusions into rivers or lakes, or determination of the thickness of the sediment layer under rivers or lakes. As stated by Bücker et al. (2020), lake sediments play a crucial role when it comes to information on the past of freshwater or the terrestrial environment. Especially sediment cores help with the reconstruction and understanding of elapsed climatological and ecological changes.

1.2 Research objectives and hypothesis

The primary objective of this thesis is to build a effective and robust floating antenna for single-loop waterborne TEM measurements. The device is used to investigate the architecture and geometry of lake-beds by measuring the electrical resistivity or conductivity of the water and the geological units underneath it. If the electrical conductivity of a water body changes, it is often an indicator for an environmental event, e.g. a saltwater intrusion into fresh water is indicated by an increase of electrical conductivity. TEM data can be used to investigate the effects of climate change on hydrogeological systems by helping find ideal coring locations for subsequent drilling campaigns for paleolimnological studies (Bücker et al. (2017)). If these materials are examined with regard to past ecological conditions, this is called a paleolimnological study. The hypothesis underlying this thesis is that TEM measurements can discriminate the contact between the surface water layer and the layer beneath it, as well as the thickness of the sediments in the lake bed. This discrimination is based on the contrast between the electrical properties that can be measured by TEM. A further aim of this thesis is to find out if a possible stratification in the lake water, in terms of its electrical properties, can be detected with TEM. To verify the hypothesis a buoyant TEM structure was used within three case studies.

1.3 Electrical properties fluid / rocks / soils

Electrical and electromagnetic geophysical methods investigate the electrical resistivity of the subsurface materials.
In general, electrical resistance is defined by Ohm's law (equation: 1.1), describing the connection of resistance R (Ω) , voltage U (V) and current I (A).

$$R = \frac{U}{I} \tag{1.1}$$

Electromagnetic geophysical methods (e.g. the transient electromagnetic method) and electric methods (e.g. electrical resistivity tomography) are all directly or indirectly measuring the electrical resistivity ρ (Ωm) of a material:

$$\rho = R * \frac{A}{l} \tag{1.2}$$

Electrical resistivity is a material property and it can be calculated as shown in equation 1.2, where R (Ω) is the resistance, l (m) is the length and A (m^2) is the cross-sectional area of the considered material (Everett (2013)).

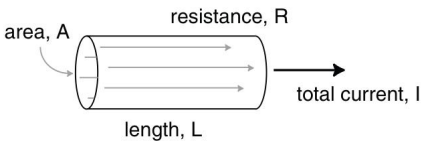

Figure 1.1: Definition of electrical resistivity. Taken from Everett (2013).

Basically electrical resistivity ρ (Ωm) or its reciprocal - the electrical conductivity σ (S/m) $\sigma = \frac{1}{\rho}$ describes the ability of a material to conduct electrical current.
Electrical resistivity of rocks and soil can be described by the different petrophysical properties, on which it depends. Those are: clay content, salinity, temperature, compaction, water saturation, pore water conductivity, porosity and clay content.

According to Kearey et al. (2013), electrical resistivity is one of the most variable physical properties. Certain rock forming materials (minerals) conduct electrical current through the passage of electrons, whereas other minerals act as insulators and electricity is carried via the passage of ions in the pore water (see Figure 1.2 for the different conductivity values regarding different materials).

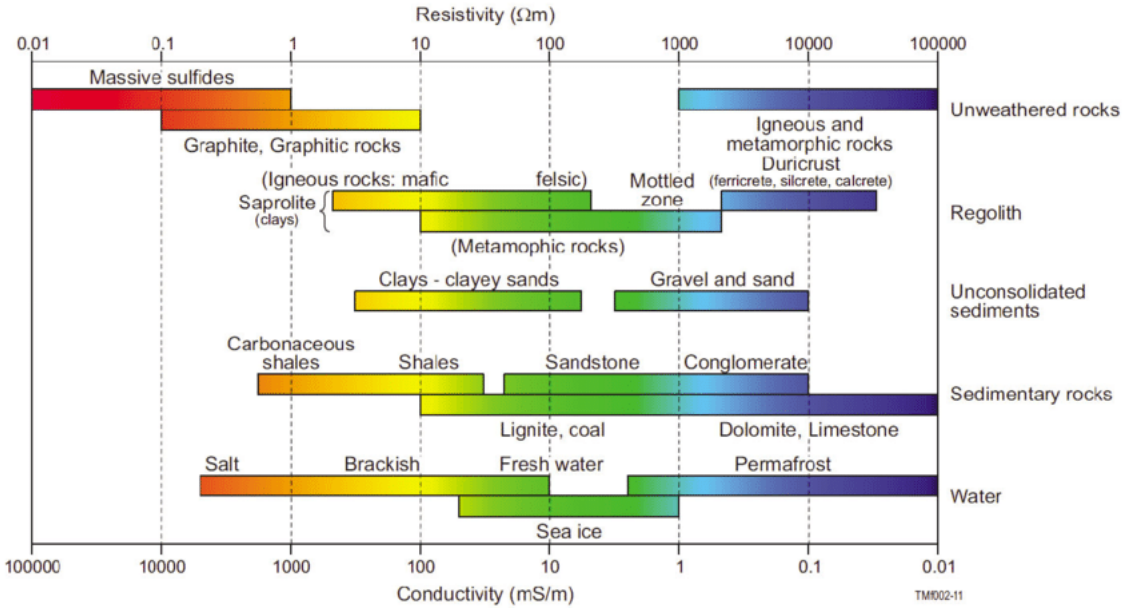

Figure 1.2: Different conductivity values for different materials, from Gonzalez-Alvarez et al. (2014).

According to Knödel et al. (2005) three different methods of conduction have been found. These methods describe how the current moves through the subsurface (see Figure 1.3):

- σ_F is the conduction of the current through the fluid in the pores
  = electrolytic conduction
- σ_A is the conduction of electrical current through the material (grains) itself
  = matrix conduction
- σ_S is the conduction of current at the surface of the material/grain surface
  = surface conduction

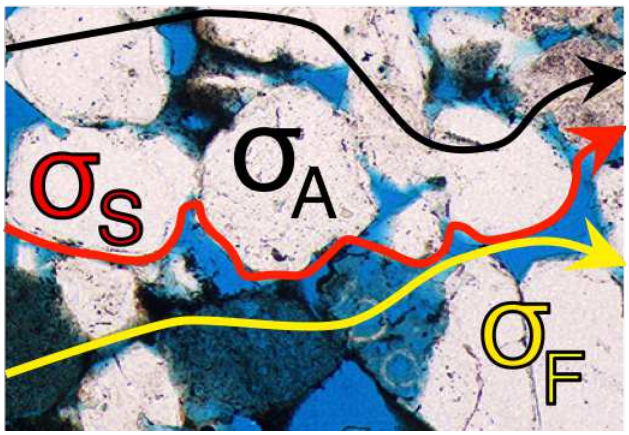

Figure 1.3: The three conduction mechanisms in a material - black describes the matrix conductivity, red the surface conductivity and yellow describes the fluid conductivity. Picture (source: grpetrology.com) modified as seen in a lecture by Adrián Flores Orozco.

Telford et al. (1990) state that the conductivity of (porous) rocks depends on their volume, the porosity, the arrangement of the pores, on the amount of water in those pores as well as on the conductivity of the pore water. Those parameters are condensed into a formula called Archie's Law (Archie 1942):

$$\sigma_0 = \frac{\Phi^m}{a}\sigma_f S^n \quad [\mathrm{S/m}] \tag{1.3}$$

σ_0 is the conductivity of the saturated rock

σ_f is the conductivity of the fluid in the pores

Φ is the porosity

m is the so called cementation exponent

a is a constant (usually a $\cong$ 1)

S is the Saturation

n is a constant (usually n $\cong$ 2)

If there are clay minerals present in the material, there is an extension to Archie's Law, because clay involves surface conductivity. When clay is present in the material, a so called electrical double layer is created, where the current will flow. According to Knödel et al. (2005) the electrical double layer is formed by the interaction of the pore fluid with the rock and causes the current to flow at the grains surface. Furthermore Knödel et al. (2005) state that this type of conductivity is connected to the clay's cation exchange capacity. Taking into account the surface conductivity, Archie's Law expands as follows (Knödel et al. (2005)):

$$\sigma_0 = \frac{\Phi^m}{a}\sigma_f S^n + \sigma_s \tag{1.4}$$

where σ_s is the surface conduction (see Figure 1.3 - red line) that originates from the clay minerals. Equation 1.4 is valid only in DC surveys.

Telford et al. (1990) proposed a classification for conductors, insulators and semiconductors. Electrical conductors are materials with a resistivity of less than 10^{-5} Ωm, insulators have resistivities higher than 10^7 Ωm and semiconductors are materials with electrical resistivity values between these two values. A difference between electrical conductors and semiconductors can be found in their different behavior in relation to temperature. Conductors are the most conductive at low temperatures whereas semiconductors are practically insulators at regions around 0 K.

Telford et al. (1990) further state that the electrical conductivity of water varies greatly, depending on the conductivity and amount of dissolved chlorides, sulfates and other minerals present. The connection of conductivity, salinity and temperature is presented in section 2.3.1.

2 Methods

2.1 TEM - transient electromagnetic method

The time domain electromagnetic method or transient electromagnetic method (TDEM or TEM), has been developed in the 1980s. It is one of the 'younger' methods in applied geophysics, according to Christiansen et al. (2006). One reason for the relatively late development of this method was the computer-intensive processing. Originally TEM was developed for mineralogical research but nowadays the focus is more on geological mapping and hydrogeological applications (Christiansen et al. (2006)), as it is the case in this thesis.

2.1.1 Physical Explanation

From a physical point of view, TEM - and all other electromagnetic methods - are based on the Maxwell equations (equations 2.1 - 2.4). These equations state the connection between electrical and magnetic fields.
An elementary electromagnetic phenomenon is that a time varying magnetic field results in a varying electrical field, which in turn generates another varying magnetic field and so on - indefinitely, according to Christiansen et al. (2006). This process of electromagnetic field propagation can be explained through the Maxwell equations.

$$\nabla \times \vec{E} = -\frac{\partial \vec{B}}{\partial t} \tag{2.1}$$

$$\nabla \times \vec{H} = \frac{\partial \vec{D}}{\partial t} + \vec{J} \tag{2.2}$$

$$\nabla \times \vec{D} = \rho \tag{2.3}$$

$$\nabla \times \vec{B} = 0 \tag{2.4}$$

∇ is the Nabla operator, $\vec{E}$ is the electric field, $\vec{B}$ the magnetic field, $\vec{H}$ is the magnetic field strength, $\vec{D}$ is the electric flux density and $\vec{J}$ is the current density vector (Christiansen et al. (2006)).

According to Yogeshware (2014), equation 2.1 and 2.2 are important for a characterisation of electromagnetic fields in terms of geophysical induction methods. However, there is no connection to earths matter or the physical properties. This connection can be made by the three following equations:

$$\mathbf{B} = \mu\mathbf{H} \qquad (2.5) \qquad\qquad \mathbf{D} = \varepsilon\mathbf{E} \qquad (2.6) \qquad\qquad \mathbf{j} = \sigma\mathbf{E} \qquad (2.7)$$

whereby μ expresses the magnetic permeability, which for most materials on earth resembles the vacuum permeability μ_0. ε describes the electrical permittivity and σ characterises the electrical conductivity of a material.
Equation 2.7 is Ohm's law for isotropic media and connects the current density $\mathbf{j}$ to the electrical field intensity $\mathbf{E}$. According to Yogeshwar (2014), this is the most relevant constitutive equation regarding geophysical induction methods.

2.1.2 Basic TEM principle

Basically, the TEM method is based on using two antennas. One is used as a transmitter and one as a receiver.
In the transmitter loop DC (direct current) circulates and is abruptly switched off. According to Faraday's law (equation 2.1) this process induces a primary electromagnetic field which propagates into the subsurface. Due to the electrical properties of the ground, currents (eddy currents) flow in the subsurface and decay with time, according to Goncalves (2012). Through this decaying current a secondary electromagnetic field is induced. This secondary field can be determined by measuring the voltage induced in the receiver loop at the surface. Figure 2.1 shows a detailed presentation of this process. An electromotive power is induced in the receiver coil. This is the signal that is measured as a function of time, according to Christiansen et al. (2006). By measuring the current in the receiver antenna, a statement about the magnetic field can be made, because these two physical quantities are proportional to one another (see equation 2.1 and 2.2). According to Christiansen et al. (2006), the secondary magnetic field contains information on the subsurface conductivity distribution. The aim is to derive this information and generate a resistivity image of the subsurface.

In Figure 2.1 (from Bücker et al. (2017)) the basic principle of TEM can be seen. The blue waveform in Figure 2.2 depicts the principle square wave of the transmitter current, whereas the red line shows the real current signal in the transmitter antenna. The current direction is shifted after each pulse to avoid influence from power lines (if the frequency of the repetition is chosen as a multiple of the usual 50/60 Hz of the power line frequency), according to Goncalves (2012).

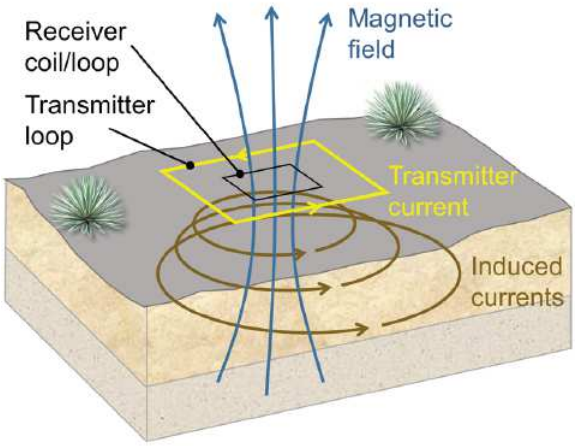

Figure 2.1: TEM basic measuring principle, from Bücker et al. 2017

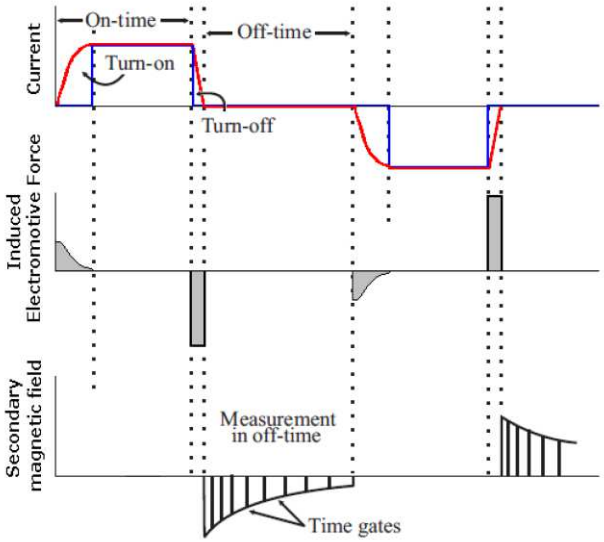

Figure 2.2: Basic TEM measuring principle - uppermost graph: current in the transmitter loop over time (theoretical current in blue, real current in red), middle graph: induced electromotive force, last graph: secondary magnetic field. Taken from Goncalves (2012).

As reported by Christiansen et al. (2006), the TEM sounding waveform consists of different stages, which have different time lengths. The 4 'stages' describe a single pulse, which is also called a transient. The four stages are: 50-200 μs for the turn-on ramp, 1-40 ms for the on-time, 1-30 μs for the turn-off ramp and 1-40 ms for the off-time. Typical TEM soundings consist of 1000-10000 transients each.

The recording of the data is done during the off-time of the current, in time windows which are also called gates, shown in the lowest part of Figure 2.2. These gates are arranged with logarithmically increasing interval time length for a higher signal to noise ratio (SNR).

The measured voltage is proportional to the change of the magnetic field over time. This magnetic field is arising from the current flow in the subsurface. The current in the subsurface depends on the resistivity of the subsurface material. Measuring at later times means measurements are done at greater depths. In summary, during the conduction of TEM soundings, the voltage in the receiver gives information about the conductivity (resistivity) as a function of depth. To get lateral information of the measuring area the loop is moved along a profile line and measurements are taken point by point.

Christiansen et al. (2006) state that the maximum of the current that is induced into the earth through the primary electromagnetic field, moves downwards and outwards in the subsurface over time (as presented in Figure 2.3). Actually, the maximum moves along a cone which creates a 30° angle with the horizontal axis, meaning that the current moves twice as much outwards than downwards (Christiansen et al. (2006)).
The magnitude is directly proportional to the conductivity (or resistivity) of subsurface materials at a certain depth. The decay of the induced current is exponential.

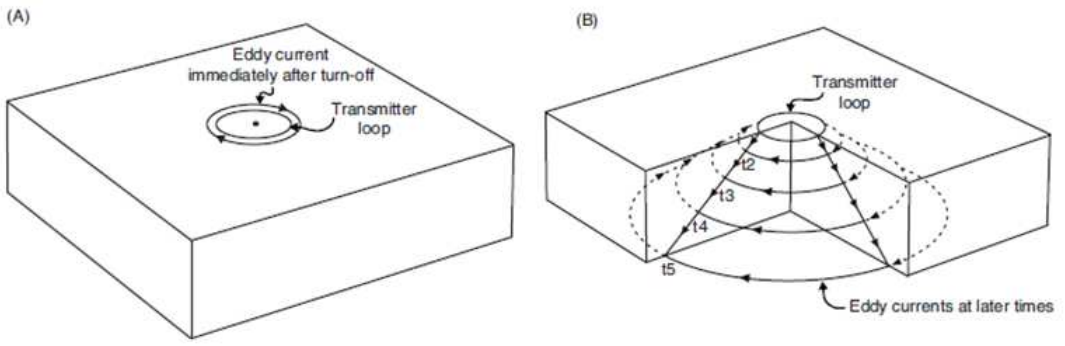

Figure 2.3: Propagation of eddy currents at early times (A) and later times (B). Currents move downwards and outwards over time, from Reynolds (2011).

The TEM measurement setup consists of a transmitter connected to a usually square shaped loop of an isolated, copper wire (usually single-turn) and a receiver loop (also made of isolated copper cable) which is connected to a receiver. Furthermore, a power supply is needed. Various configurations for the transmitter-receiver lay-out are possible, e.g. (from Nabighian et al. (1991)):

1. Single loop: One and the same wire used as transmitter and receiver.
2. Coincident transmitter-receiver loops: The same configuration as single loop set-up is used but transmitter and receiver are separate wires in a coincident shape.

3. In-loop: The receiver is located inside the transmitter loop.

4. Separated transmitter-receiver loops: Receiver is outside of the transmitter loop by a fixed distance.

5. Large fixed transmitter loop with roving receiver: Receiver measures along vertical or horizontal lines in regard to the static transmitter loop.

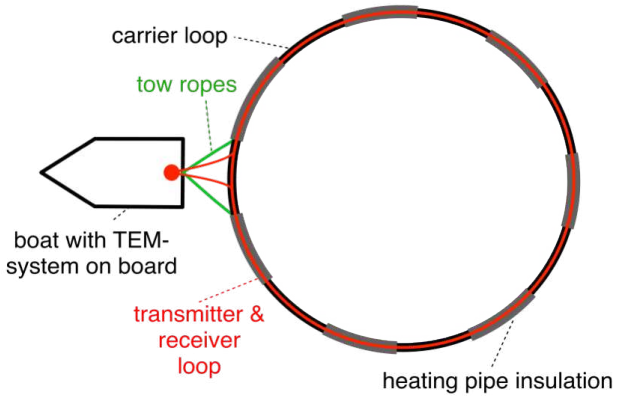

Figure 2.4: Schematic visualization of the field set up with the single loop configuration.

The single loop configuration was used in the course of this thesis (see Figure 2.4). The use of a single antenna as transmitter an receiver leads to an increase in the efficiency of the field work. The TEM-fast 48 HPC, from the company AEMR (Applied Electromagnetic Research Ltd.) was the instrument used in the course of this thesis.

Measured parameters:

According to Christiansen et al. (2006), the decaying secondary magnetic field (referred to as B) is not measured by TEM. They further state, that because an induction coil is used as receiver antenna, the actual measured parameter is the impulse response. Impulse response describes the time-varying voltage that is induced in the receiver coil.
The unit of the impulse response is Volts per square meter $[V/m^2]$. Usually the measured voltage is small - resulting in measurements of micro Volts ($\mu V = 10^{-6}V$) or nano Volts ($nV = 10^{-9}V$) per square meter, according to McNeill (1994).

When the impulse response is plotted in a log-log plot against the time, three phases of the signal can be seen. Figure 2.5 shows these three times, that are: the early time, the intermediate and the late time.
At the early time, the response is constant with time, at the intermediate time, the response shape is continually varying with time and at late times, the response is a straight line in the log-log plot according to McNeill (1994).

The impulse response is presented here for late-times (Christiansen et al. (2006)):

$$\frac{\partial B_z}{\partial t} = \left(\frac{M}{20}\right)\left(\frac{\sigma}{\pi}\right)^{\frac{3}{2}}\left(\frac{\mu_0}{t}\right)^{\frac{5}{2}} \tag{2.8}$$

M is the magnetic moment of the transmitter ($M = n * I * a^2$), which is the product of the loop turns (n) times the current strength (I) and the area covered by the transmitter loop (a^2). μ_0 is the magnetic permeability. It can be seen that the impulse response depends on the conductivity and the time. Furthermore, it can be noted that the voltage decays proportionally to $t^{-\frac{5}{2}}$ for the late-times.

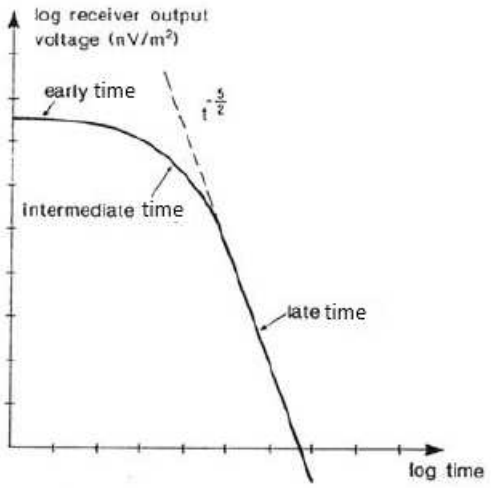

Figure 2.5: Three stages of the TEM signal, adapted from McNeill (1994).

With regards to Goncalves (2012), for each of these time ranges simple asymptotic formulas can be derived, but for the late stage the mathematics simplifies. Furthermore, Christiansen et al. (2006) propose that the parameter of the impulse response, which describes the decay of the magnetic field, may not be informative. Therefore, Christiansen et al. (2006) present a more clearer representation of the data with the late-time apparent resistivity ρ_a:

$$\rho_a = \frac{1}{\pi}\left(\frac{M}{20 * \frac{\partial B_z}{\partial t}}\right)^{\frac{2}{3}}\left(\frac{\mu_0}{t}\right)^{\frac{5}{3}} \tag{2.9}$$

Christiansen et al. (2006) state that ρ_a is derived from the late time approximation of the impulse response (equation 2.8). As shown in equation 2.9, the apparent resistivity depends on the magnetic moment (M) of the transmitter and on the impulse response ($\frac{\partial B_z}{\partial t}$).

The TEM technique is very sensitive to low-resistivity layers because the current can flow much easier in these conductive layers, according to Christiansen et al. (2006). As a result the diffusion speed depends on the resistivity of the subsurface layers. This means that the diffusion speed is proportional to the resistivity of the subsurface materials. High resistivity means high diffusion speed and low resistivity results in low diffusion speed, according to Christiansen et al. (2006).

Depth of Investigation (DOI)

As with other geophysical methods, it is also difficult for the TEM method to address a certain depth of investigation. According to Christiansen et al. (2006), for plane fields the diffusion depth z_d (corresponds to the depth to which the induced current diffuses) is described by:

$$z_d = \sqrt{\frac{2t}{\mu\sigma}}\,[m] \tag{2.10}$$

where t describes the time after current shut-off, σ stands for the conductivity of the subsurface material and μ for the magnetic permeability. Therefrom the time at which the current has diffused to the diffusion depth z_d can be expressed, which is called the diffusion time:

$$t_d = \frac{\mu\sigma z_d^2}{2}\,[\mu s] \tag{2.11}$$

When the TEM signal passes the level of natural noise, the measurement can no longer be used, as the signal strength is too weak. According to Christiansen et al. (2006) one source of natural noise are flashes of lightning from thunderstorms around the world. These lightning flashes are also called spherics. Thus, the natural noise level sets a limit for how late one can use a measurement and furthermore how deep the induced current can propagate or diffuse into the subsurface (Christiansen et al. (2006)).

An equation for the maximal diffusion depth z_d can be expressed, when the time for the latest possible measurement equals the diffusion time t_d:

$$z_d = 0.551\left(\frac{M}{\sigma V_{noise}}\right)^{\frac{1}{5}} \tag{2.12}$$

High noise level, a low magnetic moment and high resistivities decrease the depth of investigation. By analysing equation 2.12, the penetration depth can be increased either by stacking measurements to reduce the effect of noise V_{noise} on the data, or by increasing the magnetic moment M of the transmitter. This can be done by either increasing the transmitter current, transmitter area, or number of loop turns.

In summary, the depth of investigation depends on the time at which the signal decays to the noise level, on the magnetic moment and on the electrical resistivity of the earth, according to Spies (1989).

Bücker et al. (2017, p. 293) propose the rule of thumb that the depth of investigation equals 2-3 times the diameter of the loop used. This criterion can be applied during field measurements as a quick estimation.

A disadvantage of TEM is that it does not work well in very resistive media. Despite this, it is stated that the positive aspects over traditional DC resistivity measurements predominate (McNeill (1994)), which are:

- faster fieldwork
- better lateral resolution
- weight of the equipment (little more than 5 kg) and can fit easily inside a backpack.

2.2 Complementary data: ERT

The electrical resistivity tomography method (ERT) is a geophysical method that was used to get complementary data in this thesis.
Within this geophysical method, an electrical current (DC) is injected into the subsurface through a pair of grounded metal electrodes (a so called dipole) and the voltage is measured by another pair of metal electrodes. The two dipoles describe a so called four-point-measurement, as shown in Figure 2.7, where A and B represent the current electrodes and M and N represent the potential electrodes. As stated by Everett (2013), the impedance of the earth is measured. However, in this thesis only the resistivity models are considered, which are based on the inversion of the magnitude of the impedance, which is also called transfer resistance. Thus the impedance is transformed into the apparent resistivity being a more intuitively understandable parameter of the actual underlying distribution of electrical resistivity of the earth. The apparent resistivity is the quantity that allows a comparison of measurements collected with different geometries of the four-electrode array and at different positions.

According to Knödel et al. (2005), the voltage varies with the geometrical configuration used for the arrangement of the four electrodes. It also depends on the resistivities of the materials of the subsurface. The apparent resistivity can be calculated, if the ratio of the measured voltage to the injected current (meaning impedance) is known (equation 2.14). The geometrical factor K is computed as seen in equation 2.13.

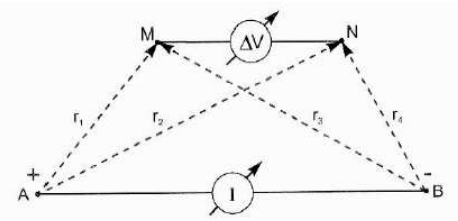

Figure 2.6: Representation of calculation for geometrical factor (from Knödel et al. (2005)).

$$K = \left[\frac{1}{2\pi}\left(\frac{1}{r_1} - \frac{1}{r_2} - \frac{1}{r_3} + \frac{1}{r_4}\right)\right]^{-1} [m] \tag{2.13}$$

For a representation of r_1-r_4 see Figure 2.6. Figure 2.8 shows the dipole-dipole configuration that was used within this thesis and the corresponding geometrical factor.

With the geometrical factor, the resistivity of a homogeneous half-space can be calculated (Knödel et al. (2005)):

$$\rho = K\frac{\nabla V}{I} \tag{2.14}$$

For a homogeneous subsurface, electrical apparent resistivity and electrical resistivity match, as stated by Bücker et al. (2017). Knödel et al. (2005) further state that because equation 2.14 is also used for any inhomogeneous conditions the term apparent resistivity ρ_a is used.

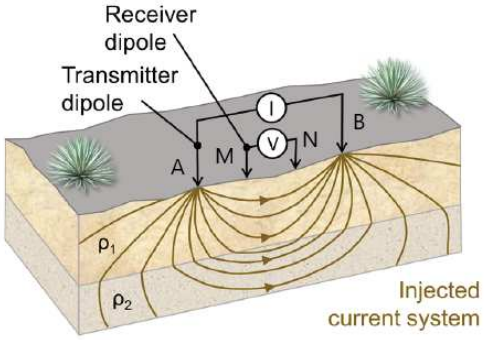

Figure 2.7: Basic principle of an ERT four-point-measurement, adapted from Bücker et al. (2017).

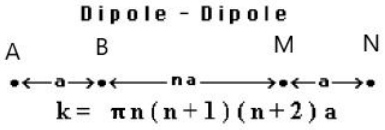

Figure 2.8: Geometrical factor for dipole-dipole configuration. A & B represent the current dipole electrodes and M & N the measuring potential dipole electrodes (adapted from Øybekk (2018)).

In nature the resistivities of materials vary horizontally and vertically. To measure the vertical variations, the distance between the electrodes can be increased gradually. Assuming that the current flows through deeper materials due to the greater distance between the electrodes used for current injection. Increasing the distance between the current and potential dipoles also increases the volume, which is sensitive in our measurements and allows us to assess deeper materials. To get information about the horizontal variations, the measurement can be conducted by moving the four-point-measurement along a profile while maintaining a certain distance between the electrodes. These two concepts are often combined and a total of hundreds of measurements can be conducted to get an image of the subsurface (Binley & Kemna (2005)). Modern measurement systems control the different combinations of electrodes automatically and are able to measure up to hundreds of different four-point configurations, according to Binley & Kemna (2005).

In this thesis, ERT has been used on water, carrying the power source (a car battery) and the measuring equipment on a boat while dragging the cable through the water (see schematic illustration in Figure 2.10). Waterborne ERT was also used by Øybekk (2018),

Rucker et al. (2011) and Huntley et al. (2017) for example. The Syscal Pro Switch 72 (IRIS instruments) was used in the course of this thesis. The main difference between waterborne ERT and on-shore ERT is the cable. A special cable, which has an additional insulation to ensure its water resistance, is used. The cable used consists of thirteen electrodes with five meters between them for a total length of 75 m. For good data quality the cable should have good contact to the water - to get the best result the cable should float a few decimetres underneath the water surface. To ensure this, heating pipe insulations were attached to the 'water cable', as shown in Figure 2.9 .

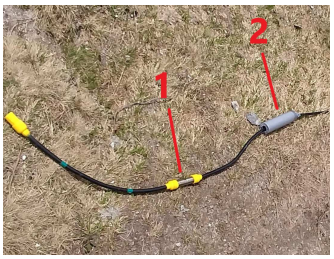

Figure 2.9: The water cable used.
(1) shows an electrode
(2) shows the heating pipe insulations used to keep the cable floating.

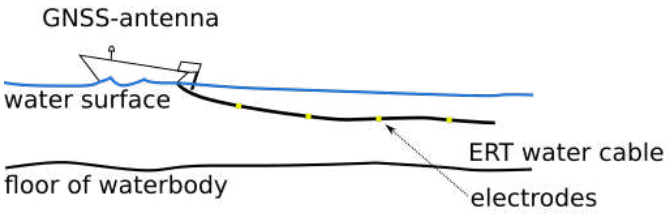

Figure 2.10: Schematic visualization of waterborne ERT measurement set up.

Similar to TEM data, ERT data has to be inverted to get a model describing the measured resistivity values of the subsurface materials (Bücker et al. (2017)). The processing of both methods is described in section 3.3.

2.3 Complementary data: CTD-probe

The CTD-probe is another complementary instrument used in this thesis. CTD stands for conductivity, temperature and depth - which are the parameters that are measured by the instrument. Its application aimed for improving the interpretation of the inversion model by providing information about the actual electrical conductivity of the water in the lake and its depth.
The probe used in the course of this thesis is called 'Aqua Troll 200 Data Logger' manufactured by the company 'In-Situ'. Figure 2.11 shows the 'Aqua Troll 200 Data Logger'. It is capable of measuring conductivity, temperature, pressure, water level (or depth), salinity, total dissolved solids, resistivity and density of water.

The conductivity measurement of the Aqua Troll is similar to the resistivity measurement done by ERT - it is also a four electrode measurement, where two electrodes are called drive electrodes and the other two are sensing electrodes. To minimize errors, AC is used and the sensing electrodes are positioned in a low current area (Aqua Troll 100 & 200

Figure 2.11: In-Situ Aqua Troll 200 Instrument, used in the course of this thesis for complementary data. Illustration taken from the Aqua Troll 100 & 200 Sonde Operator's Manual.

Sonde Operator's Manual). Conductivity is measured in Siemens per centimeter by the Aqua Troll 200 instrument.
Salinity, Total Dissolved Solids and Water Density are calculated, using either the three directly measured parameters (conductivity, temperature and pressure) or a combination of a parameter and a conversion factor.

2.3.1 Connection of Conductivity, Salinity and Temperature

Conductivity is the ability of a material to carry electrical current. In the case of water, those conductors are dissolved ions coming from solids in a dissolved form. Salts that dissolve into water are separated into positively and negatively charged ions, according to the California Clean Water Team - CWT (2004).
Salinity provides information about the amount of salts in the liquid. Salinity and conductivity are connected due to dissolved ions increasing both properties, as stated by CWT (2004).
The linear connection between electrical conductivity and salinity, that is stated in Hanson and Kaita (1997), can also be seen in the conductivity and salinity data measured at Bergwerksee near to Langau in the course of this thesis (see Figure 2.12).
In general, the electrical conductivity is directly proportional to the concentration of dissolved salts and minerals in the water, according CWT (2004). Furthermore, it is stated that deionized/distilled water acts as a poor conductor due to the lack of anions and cations which are removed in the process of deionization/distillation.

Conductivity is connected to temperature, as the value of conductivity depends on the presence of ions and their activity and as the activity and ability to move ions furthermore depends on the temperature. Conductivity meters will show different values for different temperatures. Therefore instruments should be calibrated at (nearly) ambient temperature, as stated by Katznelson R. in the DQM Information Paper.
With regards to Rhoades (1996), electrical conductivity increases at a rate of approxi-

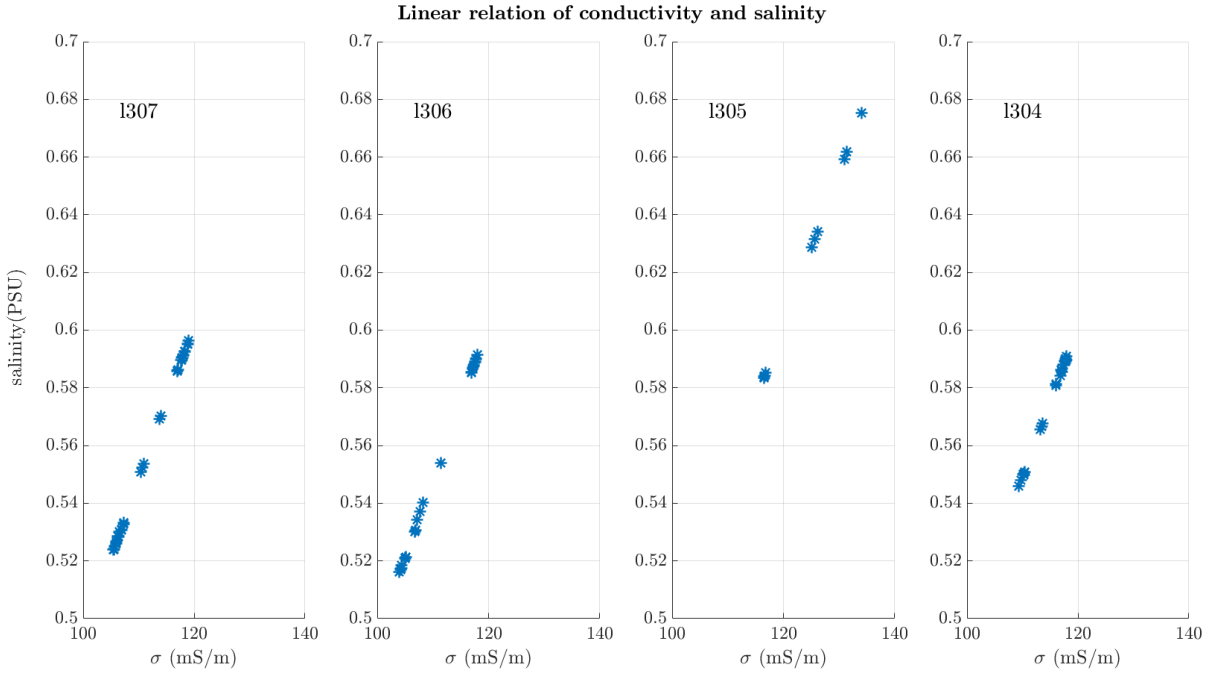

Figure 2.12: Linear relation between electrical conductivity and salinity for soundings l304-l307 from profile 3 at Bergwerksee near to Langau.

mately 1.9% per $0.1°C$. Since each ion has a different temperature coefficient, the conductivity should be measured at a temperature of 25°C for precise work.

With the CTD-probe conductivity is measured by applying a current with a given voltage between the two electrodes. The measurement is based on Ohm's law (equation 1.1). The measured parameter is the electrical conductivity. Conductivity depends on temperature, the term 'specific conductivity' is used if the conductivity has been corrected to represent the measurement temperature. As reported by the Operator's Manual of the Aqua Troll 100 & 200 Sonde, specific conductivity is an expression for the actual conductivity of a solution at a standard reference temperature (25° C).

3 Waterborne TEM

3.1 Development of the methodology

The main application of the transient electromagnetic method is on land as opposed to the field work to be covered by this thesis, which is conducted in lakes.

3.1.1 Differences between waterborne TEM and ground-based TEM

The biggest difference when using TEM on land to waterborne TEM is that the floating ring is not needed. So the set-up of the measurement on land can be done more easily, in certain circumstances even only by one person. Furthermore, less equipment is needed, which expedites the application of TEM on land. Switching to the next measuring points takes longer on land than on water because the floating structure can just be pulled to the next measurement location.
On land, the cable is put on the surface, mostly in a square shape. Pegs can be used to ensure that the shape stays stable during the measurement. Also, the position of the measurement can be determined more precisely (e.g. with GPS) because the middle of the loop can be entered, which is not the case with waterborne TEM. The measurement itself is the same procedure on land and on water.

3.1.2 State of the art

Several studies were conducted in the past, regarding off-shore or waterborne TEM, as it is called - e.g. Barrett et al. (2005), Bücker et al. (2017, 2020), Hatch et al. (2010), Goldman et al. (2004), Mollidor et al. (2013), Telfer et al. (2005) and Yogeshwar et al. (2020). These studies will be briefly reviewed in the following.

Most studies concentrated on detecting saline water influx to rivers or lakes. Barrett et al. (2005), Hatch et al. (2010) and Telfer et al. (2005) were interested in the accession of saltwater to the Murray River in Australia. All of the above used the same loop-configurations. Two single- turn square loops were used as transmitter and receiver. The size of the transmitter loop was 7,5 x 7,5 m while the receiver had a size of 2,5 x 2,5 m. The receiver loop was located in the middle of the transmitter loop. The floating frame where the wires were attached was made from timber and diagonal ropes were added to ensure stabilization while towing the antenna. They collected data while moving at low speeds along the river. The results showed that it was challenging but they could delimit the sediment layer at the river-bed.
Goldman et al. (2004) mapped saline groundwater underneath a lake. The study area

was the Sea of Galilee in Israel. In his studies he used two circular loops - a single-turn 25 m diameter transmitter loop and a multi-turn 1 m diameter receiver coil in the center of the transmitter antenna. With this approach he found that brines trapped within the sediments underneath the water are heterogeneously distributed along the lake-bed.

Yogeshwar et al. (2020) aimed to map the extent and geometry of the hydrothermal system underneath the Lagoa das Furnas in Portugal down to a depth of 200 m with an adapted in-loop configuration from Mollidor et al. (2013). The TEM system used by Yogeshwar et al. (2020) corresponded to a 18 x 18 m transmitting loop and a receiver loop of 12 x 12 m that was positioned inside of the transmitter loop in the inner frame of the construction. Furthermore, Yogeshwar et al. (2020) stated that the influence of the boat motor is negligible for the transient electromagnetic method. TEM data correlated well with the expected location of faults running through the Furnas lake system.

There have also been studies concerning paleolimnological approaches such as Mollidor et al. (2013), Bücker et al. (2017) & Bücker et al. (2020), which are described below. Paleolimnology deals with the past ecological conditions of inland waters. Climate changes, changes of the earth's magnetic field, and volcanic activities of past days can be well analyzed by paleolimnological studies. This is done by investigating the sedimentary layer underneath lakes. Core drillings are necessary to analyse those sediments. So TEM might be used to find optimal coring sites, reduce costs and help to work more efficiently.

Mollidor et al. (2013) wanted to determine the geometry and thickness of the sediment layer underneath the lake-bed of lake Holzmaar in Germany. The used TEM system consisted of a single-turn square shaped transmitter loop (18 x 18 m) and a single-turn square receiver loop (6 x 6 m) in the center of the transmitter. The elliptical form of the lake bottom caused problems for an exact estimation of the thickness of the sediments. Bücker et al. (2020) conducted waterborne TEM measurements on two lakes in Chiapas, Mexico to find optimal coring locations for paleolimnological studies. They used a single loop configuration - meaning that they used the same wire as transmitter and receiver. The loop had a diameter of 22.9 m made from PVC-pipes. One of the objectives was to see if TEM is a useful alternative to seismic methods usually used for these studies. The results showed that TEM is not a complete alternative to seismic methods but it helps with the interpretation of the data.

Figures 3.1 and 3.2 show examples for different waterborne TEM antenna configurations.

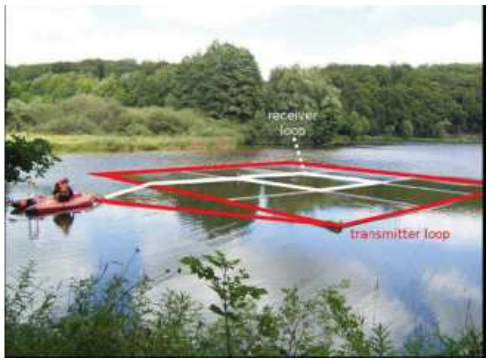

Figure 3.1: Square TEM-configuration from Mollidor et al. 2013.

Figure 3.2: Circular TEM-configuration from Goldman et al. 2004.

3.1.3 Construction of TEM-loop

For the field work of this thesis the TEM method was applied on lakes to delineate the sediment layer underneath the water and the layer below it. Furthermore, the water itself was analysed for changes in the electrical properties. Therefore, a floating construction was required to keep the TEM antenna at the surface of the water and in a permanent circular or square shape. A few requirements should be met by the construction. The construction should not be too complex, which means that it should be easy and quick to build up and should be stable enough to be towed by boat. After some research, we decided upon a circular shape and a single-loop configuration for the TEM construction (as it was used by Bücker et al. (2020)). To ensure minimum influence of side irregularities, according to Barsukov et al. (2015), a single-loop configuration was chosen. The advantage of a single-loop configuration is that no inner crosspieces are needed - just an outer ring forms the structure of the waterborne TEM antenna. With this configuration the construction is stable/flexible enough to be pulled by a boat. It is necessary to stop while conducting a measurement, since it is not possible to acquire continuous data. The construction was modeled resembling that of Bücker et al. (2020) due to concentrating on a similar research objective and aiming for an easy assembly of the floating construction. For the floating loop (seen in Figure 3.4), 15 electrical installation PVC pipes with a length of three meters each were used. The 15 pipes form a 45 m circumference when assembled. Both ends of each pipe were sealed with special foam and silicone to keep the water out. Permanent connection of the pipes during the measurement, when forces act upon the loop, was ensured by drilling holes into the ends of each pipe and putting a cable tie through the holes of two pipes put together (see Figure 3.3). To mount the cable to the floating construction, velcro straps are used during the assembly prior to measuring. Furthermore, to completely ensure the floating of the loop, heating insulations are attached to the PVC pipes. The finished construction has a radius of 7.2 m and an area

of about 161 m^2. For the field study we used a cable which was 50 m long.

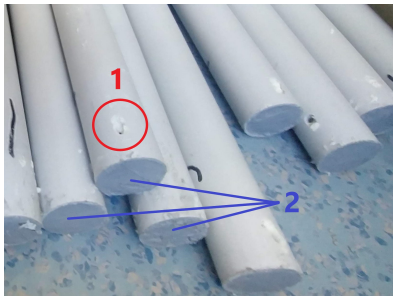

Figure 3.3: Construction of the loop.
(1) shows the holes where the cable ties are put through to ensure connection during the measurement.
(2) shows the sealing made out of special foam and silicone.

Figure 3.4: Assembled TEM-loop during field work at Laacher See, Germany.

The assembly of the floating ring should be done by at least two people. If there is enough space to enter the water, the loop can be closed on land and put to water afterwards. If there is a jetty at the lake, the loop can be built 'into' the water. In that case the end should either be attached to a rope and pulled back to the jetty to be closed or be fetched by boat and closed on the water.
During the first field test of the antenna using a motorboat (at Laacher See), the floating loop broke at the place where the loop was attached to the boat with a rope. Therefore, the PVC was reinforced at the position of the rope and two towing points were used instead of one (see Figure 3.5). Following this improvement, consecutive testing was successful and the construction was ready for the following field studies.

Figure 3.5: Improvement for measurement by using two towing points instead of one.

3.1.4 TEM instrument

The data acquisition within this thesis was accomplished with the TEM-fast 48 HPC (AEMR) instrument. The device, consisting of a single transmitter-receiver unit, battery, control unit and cables forming the loop, weighs about 5 kilograms. The TEM-fast 48 HPC is able to record data from a starting time of 4.1 μs up to 15.4 ms, after the current is shut off. 48 time gates can be used for data sampling, according to the TEM-fast 48 manual (2018). For the output current in the transmitter two options are possible - 1A and 4A. Most measurements in this thesis were done using 4A to gain a higher magnetic moment than with 1A. External power can be provided with a 12V or 24V battery. The main setting options are the transmitter current, number of stacks, length of time (corresponds to recording time), transmitter and receiver loop side length and number of turns.

3.2 Possible errors / distortions of results

3.2.1 Noise and Stacking

Christiansen et al. (2006), among others, state that geophysical measurements are never 100 % accurate. Measured data always contains both - earths response and background noise. The noise can be reduced by repeating the measurement and calculating the average of the measured signal - this process is called stacking. In Figure 3.6 the influence of stacking on the simplicity of interpretation can be seen - the black curve (5000 stacks) would be easier to interpret compared to the grey curve (50 stacks). As already mentioned, a usual TEM sounding consists of the stacking of 1000-10000 single transients.

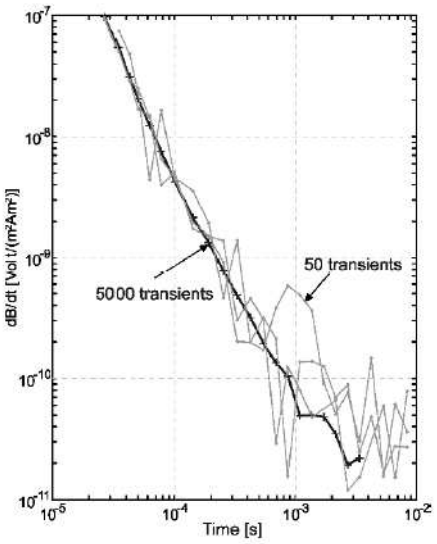

Figure 3.6: Comparison of two different numbers of stacks. Grey line - 50 transients, black line - 5000 transients, from Christiansen et al. (2006).

The mentioned background noise derives from many different sources. One major source of noise, according to Christiansen et al. (2006), are so-called spherics, which originate from flashes of lightening from thunderstorms everywhere on earth. This noise appears to be random and has a bigger influence during the daytime than in the nighttime, its influence is also greater in summer than in winter.

One man-made source of noise are the power lines, which deliver electricity to households. Their frequency is consistent and harmonic at about 50 or 60 Hz (depending on the region). Also, installations for communication (radio, TV, etc.) are going to act as a noise source. With calibrated, well working measuring equipment the noise deriving from the instrument itself should be negligible compared to the previously described noise sources.

The signal-to-noise ratio is much higher for recordings at early times. The later the times we measure, the lower the SNR is. To get data from later times it is possible to either, as mentioned above, use stacking to increase SNR or increase the moment of the transmitter. According to Christiansen et al. (2006), stacking reduces the Noise proportionally to $\sqrt{N}$ (N... number of measurements in the stack). The magnetic moment can be increased by either increasing the number of turns of the antenna, increasing the size of the antenna or by increasing the transmitter current.

3.2.2 Coupling

Coupling, according to Christiansen et al. (2006), describes the effect, when current is induced into all kinds of man-made structures that act as electrical conductors (see Figure 3.7). These structures need to be in the same area where the generated magnetic field propagates to produce noise for the measurements.
All soundings have to be evaluated individually to detect possible coupling effects in the measured data. If affected data sets are identified, they have to be removed before the inversion is performed. A safe distance, meaning a minimum distance where good data can be measured (Christiansen et al. (2006)), should be kept to man-made structures.

Coupling types:

- Galvanic Coupling is usually difficult to identify, because the affected sounding curve is just shifted. Triggers for galvanic coupling could be high-voltage power lines (see Figure 3.7 (a)).
- Capacitive coupling is normally easy to recognize because of its oscillating form. Sources for capacitive coupling could be buried cables (see Figure 3.7 (b)).

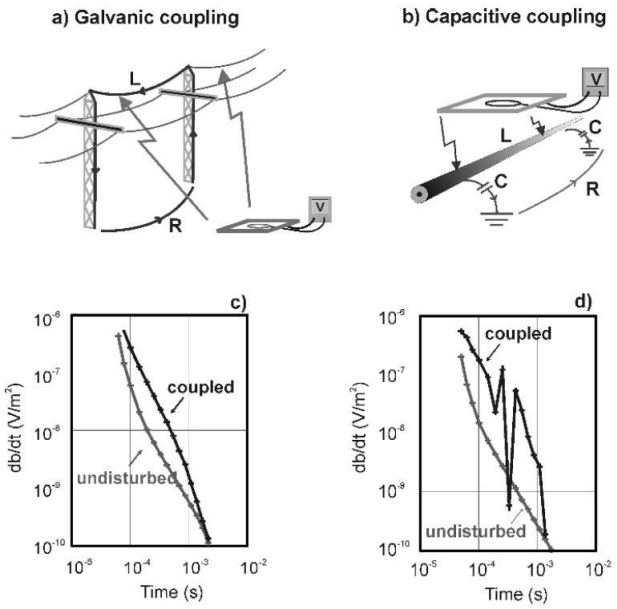

Figure 3.7: Coupling types and their effects on the data from Christiansen et al. (2006). Capacitive coupling creates an oscillating signal, which can be determined easier than the shift of the signal that is generated by galvanic coupling.

3.2.3 Influence of different cables

A question to be answered before starting with the measuring campaigns was whether the measurement is affected by the type of the cable used.
Therefore, different cables were tested and the recorded data was compared to investigate a possible influence from the cable on the measurements. No coupling could be observed and previous measurements revealed a good SNR for the area where the tests were carried out on the Donauinsel in Vienna.
The tested cables vary in length, thickness (or cross section area) and hence in resistance (measured by multimeter). The cable properties can be seen in table 3.1 for circular loops. As transmitter current 4A were used. A stack setting of 10 and a time interval from 4 μs to 64 μs were used. For the sampling of the signal 16 time gates were active after the current was shut off.

type of cable	loop circumference [m]	cross section area (mm^2)	resistance (Ω)
50 m cable (cable 1)	45	0.5	1.83
45 m cable (cable 2)	39	2.5	0.60
50 m cable (cable 3)	45	0.5	2.05
45 m cable (cable 4)	39	0.5	1.75

Table 3.1: Differences in used cables.

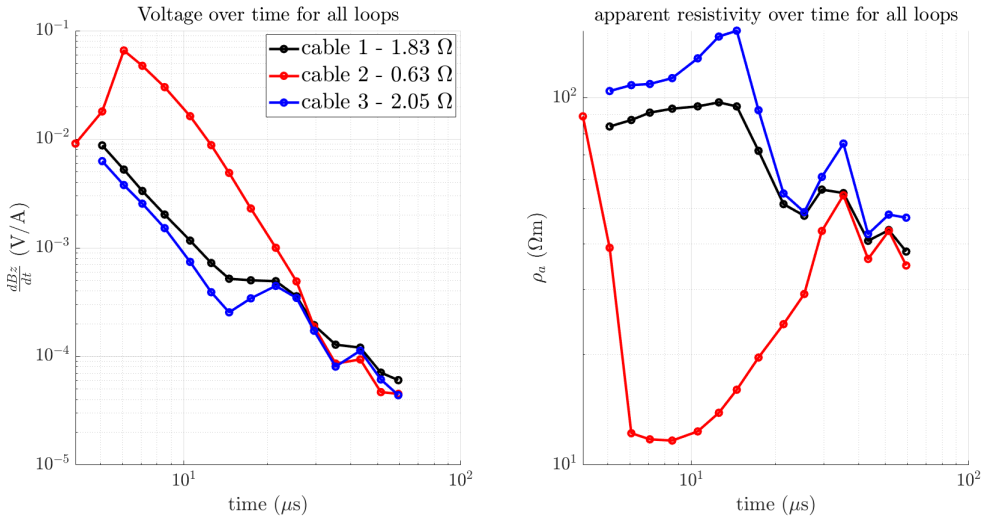

Figure 3.8: Raw data visualization for cables - see list above for cable properties.

The raw data is plotted in Figure 3.8. A clear difference can be seen in the course of the recorded data curves for the different cables. Usually, one would expect the curves of the cables with different lengths to show similar or - to put it another way - shifted curves depending on the magnetic moment of the measurement-set up. This can be seen when looking at the black and blue (representing cable 1 and cable 3). The signal from those two cables look alike. The red line on the other hand looks different. It is assumed that this behaviour stems from the lower resistance of cable 2 compared to the other two. With regards to Barsukov et al. (2015), the voltage in a loop at early times depends on its resistance, its size, its capacitance and inductance. Therefore, the choice of cable used is important. For the measurement in this thesis, cable 3 with a length of 50 m was chosen.

3.2.4 Influence of different loop shapes

Apart from the choice of the used cable, another point of interest was how the shape of the transmitter/receiver loop influences the registered signal. Therefore, different shapes of loops were tested and the measured signals are compared in this section. The three shapes were a single turn square, a single turn circle and a double turn circle. The transmitter circumferences were 45 m for the single turn circle, 50 m for the square and 90 m for the double turn circle. The area covered by the transmitters were: 161.1 m^2, 165.3 m^2 or 644.6 m^2. As transmitter current 4A were used. A single stack and a time interval from 4 μs to 256 μs were used. For the sampling of the signal 24 time gates were active after the current was shut off.

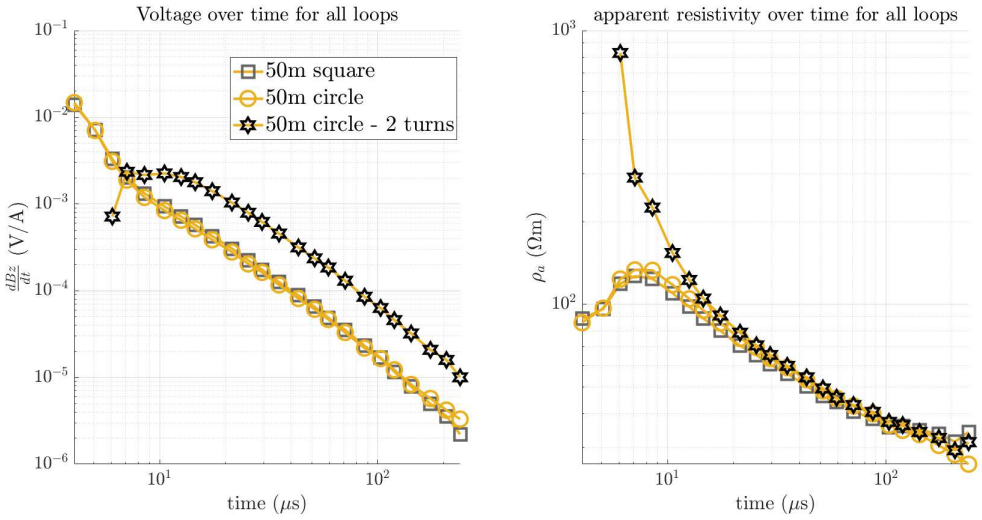

Figure 3.9: Raw data visualization for cable 3 (50 m long) used for the waterborne TEM measurements, described above. For the testing, different antenna shapes were used. Additionally, a comparison with a 2 turn antenna was done.

In Figure 3.9 three different laying of cables are shown. It is shown that the double turn antenna (marked by stars) has the biggest signal response due to it having the biggest magnetic moment. The curves for the other two shapes are similar despite the circle having a larger area, which should therefore have a bigger magnetic moment. It is assumed however, that the difference in area is too small for this scale to have a significant influence on the resulting data. The shape of the transmitter loop defines the area covered by the antenna. This has an influence on the magnetic moment and thus on the SNR and the depth of investigation.

3.2.5 Influence of the Ramp Effect

The influence of the turn-off ramp affects the readings at the early times. The ramp effect is one of the reasons for the lower resolution of TEM for the shallowest investigations compared to the deeper parts of the subsurface.

The current in the transmitter loop is assumed to be shut off as a step function but actually, according to Raiche (1984), the turn-off signal is more similar to a ramp function (as presented in Figure 2.2). Ignoring this fact can lead to errors in the first few layers, which is also stated by Fitterman et al.(1987).

The TEM-fast 48 HPC instrument that was used for the field measurements in the course of this thesis has an On-Time from 0.23 to 67.2 ms while the Off-Time ranges from 0.08 to 22.5 ms.
During the data processing, it was common to eliminate the earliest data points. With a quantification of the turn-off ramp (time) its issue should be removed and the data curves should be corrected using the right ramp-time for the inversion process.

To quantify the ramp-turn-off time, an oscilloscope ('Voltcraft - DS - 1084F') was used to measure the signals within the transmitter loop while the TEM-fast-device is running a measurement. The measuring was done at the Donauinsel in Vienna. The evaluation of the turn-off ramp was realized following the methodology by Aigner (2019).
The first peak, represented in Figure 3.10 on the right side, can be linked to the electromotive force caused by the current switch-off process. The width of this peak, which corresponds to the width of the induced electromotive force peak, presented in Figure 2.2, was used to determine the length of the turn-off ramp. In Figure 3.10 on the right side, the ramp time equals the difference of t_2 and t_1. Where t_1 represents the point in time when the current is shut off, and t_2 the time when the current reaches the initial signal level.

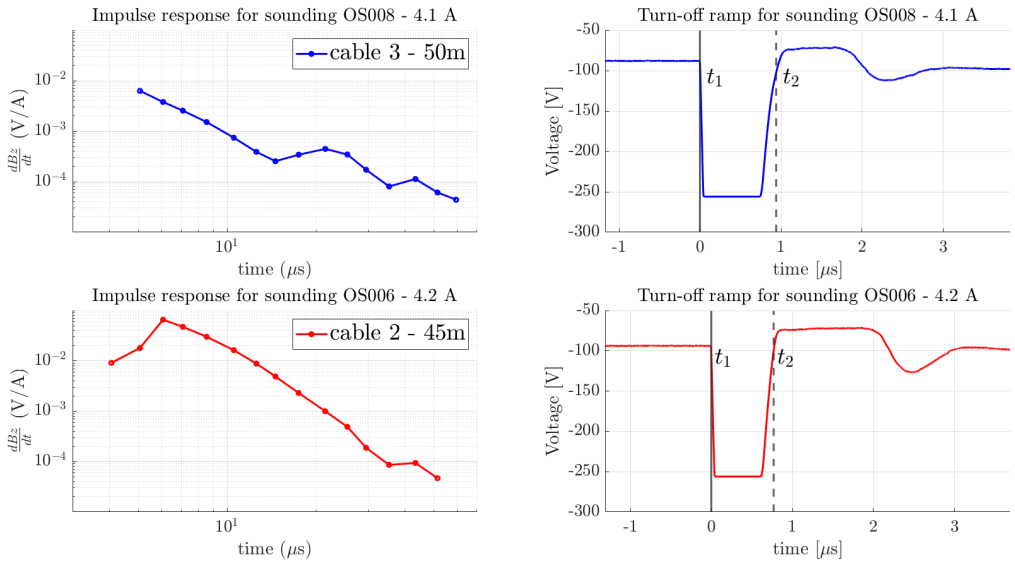

Figure 3.10: Left side: Impulse responses for cable 3 (50 m) and cable 2 (45 m). Right side: Graphic representation of ramp calculation.

The oscilloscope measurements were done for two cables, which were used in this thesis. The calculated ramp-times for 4A measurements are shown in table 3.2

type of cable	cross section area (mm^2)	resistance (Ω)	ramp times (μs)
50 m cable (cable 1)	0.5	1.83	0.96
45 m cable (cable 2)	2.5	0.60	0.77
50 m cable (cable 3)	0.5	2.05	0.94
45 m cable (cable 4)	0.5	1.75	0.84

Table 3.2: Extension of table 3.1 by ramp time values.

The calculated time-values can be set within ZondTEM1d under the tab 'station settings' - 'time mode', as shown in Figure 3.12.
Raiche (1984) also states that preliminary work indicates that the ramp turn-off time is affected by the top layer resistivity. The author suggests recording the source waveform in the field whenever possible.

3.3 Processing and inversion of geophysical data

3.3.1 General processing

The basic processing of geophysical data consists of 4 main steps, which are:

1. Visualization of raw data
2. Filtering and elimination of incorrect data
3. Inversion of data
4. Interpretation of inversion results

(1.) Raw data visualization is important for getting a first impression of the quality of the measured data. It also provides information for a following comparison of the data after the filtering process.

(2.) Elimination of incorrect data describes the process of removing bad points from the data set. Filtering corresponds to advanced data processing.

(3.) The inversion step, which is addressed in more detail in section 3.3.3, describes the process of searching a model that describes the measured data best.

(4.) The inversion model is then checked against known information about the study area, which may have been generated through additional/complementary geophysical methods. Furthermore, interpretation of the resulting model can be done and a preliminary conclusion is presented.

3.3.2 Processing of TEM data

TEM data can be processed individually or all soundings of a profile at once. The steps for both types are similar. The analysis of several soundings at once is done to enhance the comparison of inversion results along sections.
During the first step - the raw data visualization - the data curves are checked for visible data errors. These errors can arise from different sources - which are described in more detail in section 3.2.
Both, the measured signal (or impulse response) and the apparent resistivity are visualized in this step. The curves are assumed to decay smoothly with time, whether impulse response or apparent resistivity. The shape of the curves can be checked in this step.

If the curve does not look smooth, this could stem from negative voltage readings. Therefore, they need to be removed. The negative transients in coincident or single loop configurations (as it is the case in the fieldwork in this thesis) can be attributed to noise as well as to polarization effects, according to Marchant (2015). The induced polarization effect is not further elaborated in the context of this work but it is comprehensively described in works by Goncalves (2012) and Marchant (2015). Data points that are disturbed by this effect are simply removed from the curve as they are assumed to be incorrect. When removing the negative data readings, not only the negative data point needs to be eliminated, but also the readings before or after this erroneous datapoint to obtain data consistency. The decision whether to delete points before or after the negative data reading depends on its position in the curve. If the erroneous data reading occurs in the first third of the curve, all points before it are deleted (including the negative one). If it arises in the last third, all points after the error are deleted.
For the unusual case when multiple voltage readings with a negative sign arise along the whole sounding curve the whole sounding can be rejected.
After this first filtering there should only be data curves left, where the signal decays evenly with time, as it is assumed in the beginning. If there are still discontinuities in the data, which make the curves look rough, those data points are treated equally as the negative readings in the step described above and are removed (as well as the values before or after the point that differs from the overall smooth looking curve).
Furthermore, all data curves are cut to the same low noise time interval to enhance comparison. This means that all soundings are cut at a given time to remove readings with low SNR. The filtering and truncation, described above, was done using MATLAB.

Following the filtering step, a first test inversion is run. (The inversion process is described in detail in section 3.3.3)
If the fitted curve aligns well with the measured curve and the data fit is acceptable, the inversion is finished here. If this is not the case, this means that the data fit is inadequate. Then data points can be removed either from the front or the back of the curve. Where to remove the data points depends on the location of the bigger misfit. This process is repeated iteratively, if the data fit is still not in an acceptable range after another inversion. This process can be repeated until the data fit takes on a desired value that is decided by the user but should be under 10. Another result could be that removing points leaves less than 5 data points for a given sounding. If this is the case, no meaningful result can be obtained. Then the sounding should either be discarded, another start model should be chosen or the inversion parameters should be altered.
The inversion and removal of single data points was done in ZondTEM1d, which permits

a simultaneous visualization of the filtering and modeling result.
There is always the possibility of removing a single sounding entirely, if a certain data fit level cannot be reached through the inversion process or even if no model can be found to describe the data.

3.3.3 Inversion

A geophysical Inversion is an iterative process to obtain a model of the subsurface which best describes the measured data (schematic representation in Figure 3.11). More precisely the geophysical inversion refers to statistical and mathematical techniques to gain information about physical properties of the subsurface from measured data (e.g. J. Reid (2014)).
In the first step the inversion algorithm computed the forward modeling to calculate the model response (i.e. synthetic data) from an initial subsurface distribution of the electrical resistivity. The model response of the start model is compared to the observed (i.e. measured) data. If the difference is bigger than a certain threshold (i.e. root mean square (RMS) error), the model parameters of the initial model are altered and the forward calculation is repeated. Then another comparison between the model response and the measured data is done. This process will be repeated iteratively until a certain abort criterion is met (e.g. a specific number of iterations or a certain threshold). This means that many models are created consecutively and the one which best fits the data will be chosen as a representative (Reid (2014)).
In the case of the TEM method observed data is the impulse response (i.e. the decay of the voltage over time), whereas for ERT the data is the measured potential difference (i.e. voltage and the calculated resistance).

According to Goncalves (2012), 3 steps are necessary to solve the inverse problem.

1. Parameterize the model (divide the study area into discrete regions of uniform properties)

2. Find relationships between model parameters and observed data

3. Apply a method that finds the closest model response to the observed data . This is done via a minimization of the difference between the measured data and the calculated values from the direct problem.

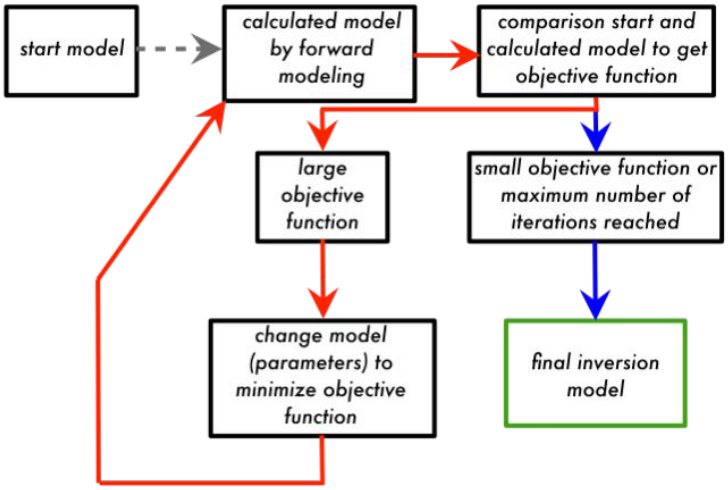

Figure 3.11: Basic principle of an inversion. Iterative process (red arrows) until a certain abort criterion is met, adapted from Reid (2014).

There are two main problems regarding the inversion process:

- ambiguities/non-uniqueness - there is not only a single model which can explain the measured data.
- instability - small changes in the data can result in a big impact on the solved model.

The goal of the inversion process is to find the smoothest model that describes the measured data.

Parameters and execution

The inversion for TEM data in the course of this thesis was done with the commercial software ZondTEM1d (by Alex Kaminsky (2001)). The calculated ramp time was set to the calculated value before starting with the inversion process in ZondTEM1d (shown in Figure 3.12). Additional pre-processing steps were done in ZondTEM1d prior to the inversion. The graphical user interface permitted to delete single points in the early or late times to obtain an improved fit for the calculated data to the measured data. The initial model was created either with the user interface in ZondTEM1d (if one start model was used for the whole set of soundings) or with a MATLAB-script (if each sounding uses an individual start model). The depth of the start model was calculated using the rule of thumb described by Bücker et al. (2017, p. 293), after which the DOI equals 2-3 times the

diameter of the loop. Before starting the inversion a few parameters could be changed in the graphical user interface of ZondTEM1d (shown in Figure 3.13 and described below).

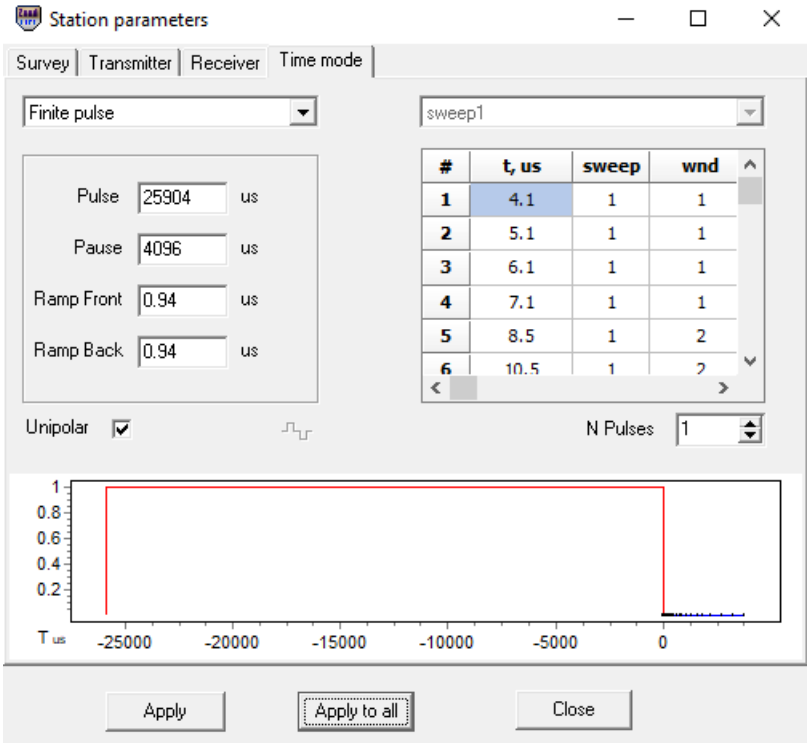

Figure 3.12: Tab in ZondTEM1d to control the ramp-parameters.

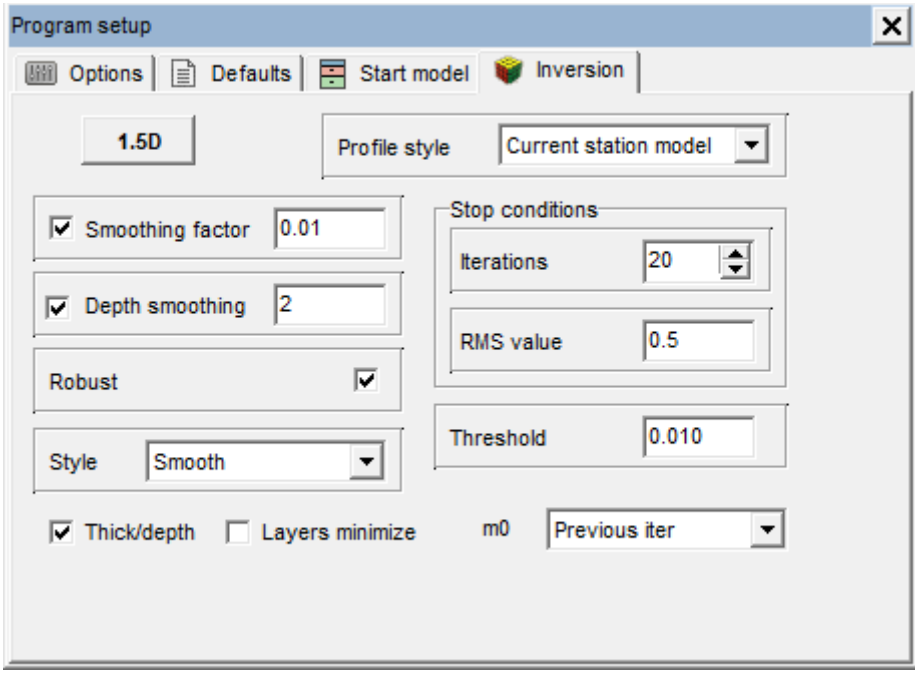

Figure 3.13: Settings for the inversion in ZondTEM.

Some of the most important parameters are (explanations from ZONDTEM1d manual):

- Profile Style: Adjusts the inversion style for profile inversions - three possibilities :
  - *current station model* - the current station model is used as initial model for the inversion (this option was always selected in the following case studies).
  - *start station model* - model of the start sounding is used as initial model for all points.
  - *previous station model* - previous station model is used as initial model for the inversion.
- Smoothing factor: This parameter aims at reducing the instability in the inversion by forcing a smooth response and remove the effect of possible outliers in the data. In case of a clean decay curves it is possible to reduce such parameters. In our case we select a value of 0.01 for the work in this thesis.
- Depth smoothing: sets the degree of smoothing of the model depth. The larger its value is (1 - 10), the more parameters of adjacent layers are averaged with depth. This option can only be used with the style setting *smooth*.
- Style: Sets selection for recovery of section parameters.
  - *Smooth* - Inversion by least-square method using a smoothing operator. This selection results in the smoothest parameter distribution, as stated in the ZondTEM1d Manual. This was also the option that was mainly chosen in the case studies.
  - *Standard* - Inversion by least-square method using a damping factor regularization (ZondTEM1d Manual) . Results in a model with sharp boundaries.
  - *Focused* - Inversion by least-square method using a smoothing operator and additional contrast focusing. This allows sharp contrasts (e.g. water - lake bed) and still smooth transitions in each of the two blocks. The number of layers in the model should exceed the number of layers in reality to get a reasonable model, according to the ZondTEM1d Manual.
- layers minimize: Minimizes number of layers by merging layers with similar parameters and the inversion process continues with a lower number of layers. This setting is usually used with a start model of 10-15 layers and *focused* inversion.

- Stop conditions: Define when the inversion stops, meaning that the inversion process is finished, when one of the two entered values is achieved
  - *Iterations*
  - *RMS value*

Further details can be found in the ZondTEM1d Manual.

All soundings within this study were inverted using the following settings:

- **profile style:** current station model
- **style:** smooth
- **threshold:** 0.01
- **smoothing factor:** 0.01
- **depth smoothing:** 2
- **stop conditions:**
  - **iterations:** 20
  - **RMS:** 0.5

Constraint Inversion

A possibility to include known information into the inversion process and to reduce both the non-uniqueness and instability is to include a-priori information about the subsurface as structural constraints. Such constraints can result in dramatic improvements of the resulting inversion model. Constraint information for the inversion model parameters are considered constants, according to Menke (2012).
In this thesis, depth and electrical resistivity of the water were often used as constraints. A known problem with electrical and electromagnetic geophysical applications in water is that the current tends to flow only in the water. This is due to the conductivity of the water being (in most cases) higher than the conductivity of the layer below the lake bottom. This disadvantage is often circumvented by measuring the depth and resistivity of the water layer independently and using the data as a-priori information (or constraints) in the following inversion, as stated by Butler (2009).

3.3.4 Processing and Inversion of ERT data

The steps of ERT data processing principally match the general processing procedure. The processing starts with the visualization of the raw data, which can be done with a so called pseudosection. According to Everett (2013), a pseudosection is a representation of the apparent resistivity in different depths and lateral positions.
In the pseudosection it is often possible to detect obvious outliers (e.g. non connected electrodes) and eliminate them in a further step.
After the following filtering step, the data is inverted. The inversion uses the principle as described in section 3.3.3.

The ERT data was processed using the open source programming language Python. Within Python the packages matplotlib and pyGIMLI (Rücker et al. (2017)) were used for processing, inversion and visualization of the ERT data. To limit the scope of this work, scripts from Lukas Aigner and Nathalie Roser were used. The scripts were adapted to fit the needs for the processing and inversion of the ERT data. Visualization of the inversion results was also done using Python.
The input parameters for the inversion were:

- the observed data
- a mesh defining the discretization and geometry of the resulting model
- the absolute error (err_{abs}) in Ωm
- the relative error (err_{rel}) in %
- the regularization parameter λ
- z_{weight}

According to Flores-Orozco et al. (2012), the final inversion result strongly depends on the data error and its parameterization. Therefore, the data error for the inversion needs to be quantified based on the actual readings. This is done via an error model that relates the measured resistances with their associated errors (err_{abs} and err_{rel}).
The regularization parameter λ weighs between data closeness and model roughness, according to Yogeshwar (2014). Large values for λ lead to smooth models and a bigger data misfit, whereas small λ values lead to rougher models and smaller data misfit. It can be stated that a compromise between model roughness and data misfit should be made (Yogeshwar (2014)).
z_{weight} is a smoothing parameter. According to Günther and Rücker (2015), its value defines the relative weight for a purely vertical border. Values between [0-1] are allowed.

Small value result in horizontal smoothing and large values result in vertical smoothing.

The ERT inversion result consists of the inversion mesh and a corresponding resistivity vector (i.e. one value for each mesh sell), as well as a sensitivity vector. The sensitivity can be used to blank parts of the resulting model in areas where the modelled values are not sensitive to the measured data.
The values for the inversion parameters used in this thesis were:

- $err_{abs} = 0.001\ \Omega m$
- $err_{rel} = 0.1\ \%$
- $\lambda = 500$
- $z_{weight} = 0.5$

4 Results

4.1 Case Study 1: Identification of changes in water properties (Laacher See)

4.1.1 Introduction

The Laacher See, a volcanic lake, shows interesting seasonal changes of water properties. A layering of the lake water in terms of electrical properties is known to appear during summer time and does not occur in the winter months.
According to Aeschbach-Hertig et al. (1996), vertical water exchange in summer is limited because of thermal density stratification. In Aeschbach-Hertig et al. (1996) measurements from summer 1991 show a remarkable thermocline, which is a layer where water temperature changes more intensely with depth than in adjacent layers. A chemocline, which is a thin layer where chemical properties change drastically and which can be determined by electrical conductivity (Aeschbach-Hertig et al. (1999)), might also be present in Laacher See. In their study, Aeschbach-Hertig et al. (1996) show that such a thermocline is located in Laacher See in about 8 to 15 m depth across the whole lake (shown in the top plot of Figure 4.2). The thermocline divides the water in a well-mixed upper, warmer surface layer also called epilimnion and a vertically stratified deeper layer with cooler water called hypolimnion (Aeschbach-Hertig et al. (1996)).
Two campaigns were conducted at the Laacher See aiming to investigate whether TEM is able to detect changes in water properties, specifically to show the stratification of the water in terms of conductivity and temperature. The geometry of the layers, i.e. the thickness and possible lateral variations should also be investigated. Aeschbach-Hertig (1996) states that, in terms of temperature and electrical properties of the water column, this layering does not occur in winter. During both field operations waterborne ERT measurements and CTD measurements were conducted to validate the TEM results and aid in their interpretation. In a second step, this additional information was used as a-priori information to improve the inversion of TEM data. Furthermore, the measured data was shared with other research teams.

4.1.2 Study Area

The two measuring campaigns took place in late August 2019 (19th - 23rd) and in early March 2020 (9th - 12th). Laacher See is located in the so called Eifel Volcanic Field in the state Rheinland-Pfalz, approximately 40 km south of Bonn in Germany. According to Aeschbach-Hertig et al. (1996), the craters (called maars in the Eifel fields) were formed as a result of steam explosions, which occurred when water came into contact with a magma chamber near the surface. Some of those maars formed lakes - one of them is Laacher See, which is actually the largest maar lake in Germany. The lake was formed because of an volcanic eruption 11.000 years ago. The lake in the Laacher See caldera covers 3.31 km^2 and has a maximum depth of 52 m according to Aeschbach-Hertig et al. (1996).

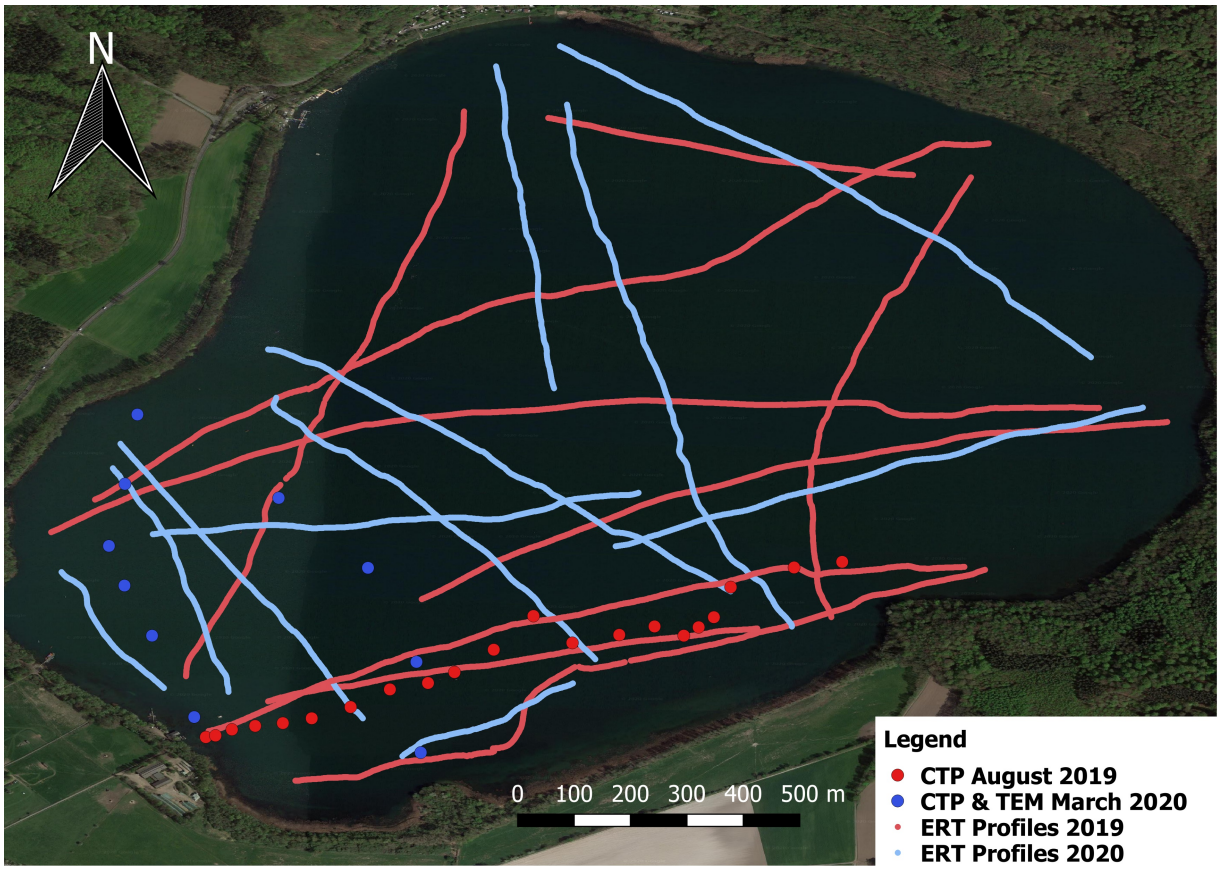

Figure 4.1: Overview of the measuring area at Laacher See from the campaigns in August 2019 and March 2020. TEM-soundings were collected at the same locations as the CTD sites. Due to strong winds during the campaign in march 2020, TEM/CTD measurements were only possible at the western side of the lake, which is sheltered by the caldera.

The equipment used for both measurement trips were the 'TEM-fast 48 HPC' (manufactured by AEMR) and the 'Syscal Pro Switch 72' (manufactured by IRIS Instruments). For the first campaign a CTD probe from the university of Bonn was used to measure the electrical conductivity and temperature of the water. The readings were written down

manually because the probe was not able to store the readings automatically. For the second campaign in March 2020 the 'Aqua TROLL 200' (manufactured by In-Situ) was used. It samples each second and is able to automatically store the data.

The waterborne-TEM soundings were collected using a circular loop with a radius of 7.2 m and an area of 161 m^2. The cable used to form the circular loop is 50 m long. As transmitter current of 4 Ampere was injected in the cable to generate the primary field. A single stack and a time interval from 4 μs to 4096 μs were used. For the sampling of the signal 40 time gates were active after current shut-off. This set-up allows for a depth of investigation of about 35 m. During the measurements the loop was separated from the boat by 2.5 m. The water cable described in section 2.2 was used for the waterborne-ERT measurements. The dipole-dipole configuration was used for the ERT profiles.

In August 2019, 62 TEM soundings were conducted, 11 ERT profiles and 21 CTD points along TEM profile 2 were measured (shown in Figure 4.1 in red).
While processing the TEM data from the first measuring campaign, physically implausible readings were observed. These signals show an increase of the impulse response with time. After some discussions about the data and tests of the device, we discovered that the device was damaged, although it seemed to work perfectly fine during the field trip. The device was posted for repairs later on and for this reason no TEM data from the first field work of this case study (in August 2019) is presented in this thesis. Thus, only ERT and CTD probe data was processed from August 2019 and is discussed in this section.

The second survey was conducted between 9th and 12th March 2020. The TEM device was working again and the measurements could be carried out as planned.
During the two measuring days in March 2020, 15 TEM soundings were conducted. Additionally, 11 ERT-profiles and 10 measurements were carried out by the CTD probe, to verify the quality of the measurements and the results (shown in Figure 4.1 in blue).
CTD-probe measurements were used to gain a-priori information for the inversion process of the TEM and ERT data. CTD probe measurements were obtained at the exact same locations as the TEM soundings. The TEM measurements were split into two profiles, the first one from P01-P05 and the second from P05-P15 (presented in Figure 4.1 - the eastern blue points refer to the P01-P05 profile, whereas the western blue points present the P05-P15 profile).

Because of strong winds and the TEM-structure being too fragile to steer the boat at greater speeds, we could not cover the whole lake for a TEM-mapping. Therefore, only

soundings in the southwestern part of the lake exist, where the wind affected the navigation less than in other parts of the lake. With the help of ERT it was possible to conduct measurements across the whole lake, as the ERT cable is more stable, which makes it possible to measure at higher speeds. While using TEM 3 km/h were not exceeded, whereas with ERT 5 to 6 km/h were no problem.

4.1.3 CTD data

Figure 4.2 presents the CTD data collected at Laacher See along two profiles, one during the first campaign in 2019 and the other during the second survey in 2020.
The localisation of the measurement points are presented in Figure 4.1, where the 2019 points are colored in red, the 2020 measurements in blue.
Figure 4.2 shows the temperature data from the CTD probe in the top two plots. The thermocline can be seen in a depth of about 10 m in the first plot (showing the data from August 2019). No stratification of the water can be seen in the CTD temperature data of March 2020 (second plot in Figure 4.2).
The lower two plots in Figure 4.2 show the conductivity data collected with the CTD probe at Laacher See during the two measuring campaigns in 2019 and 2020. The chemocline is also clearly visible in the conductivity data from summer 2019 (third plot in Figure 4.2). The chemocline can be seen at a depth of about 10 m. No layering in terms of electrical conductivity can be seen in the CTD data from March 2020 (fourth plot in Figure 4.2).
An echo sounder was available during the survey of 2020 and water depth was noted at every CTD measuring point. That was not the case for the field trip in August 2019, resulting in no depth data at the CTD measuring points there.

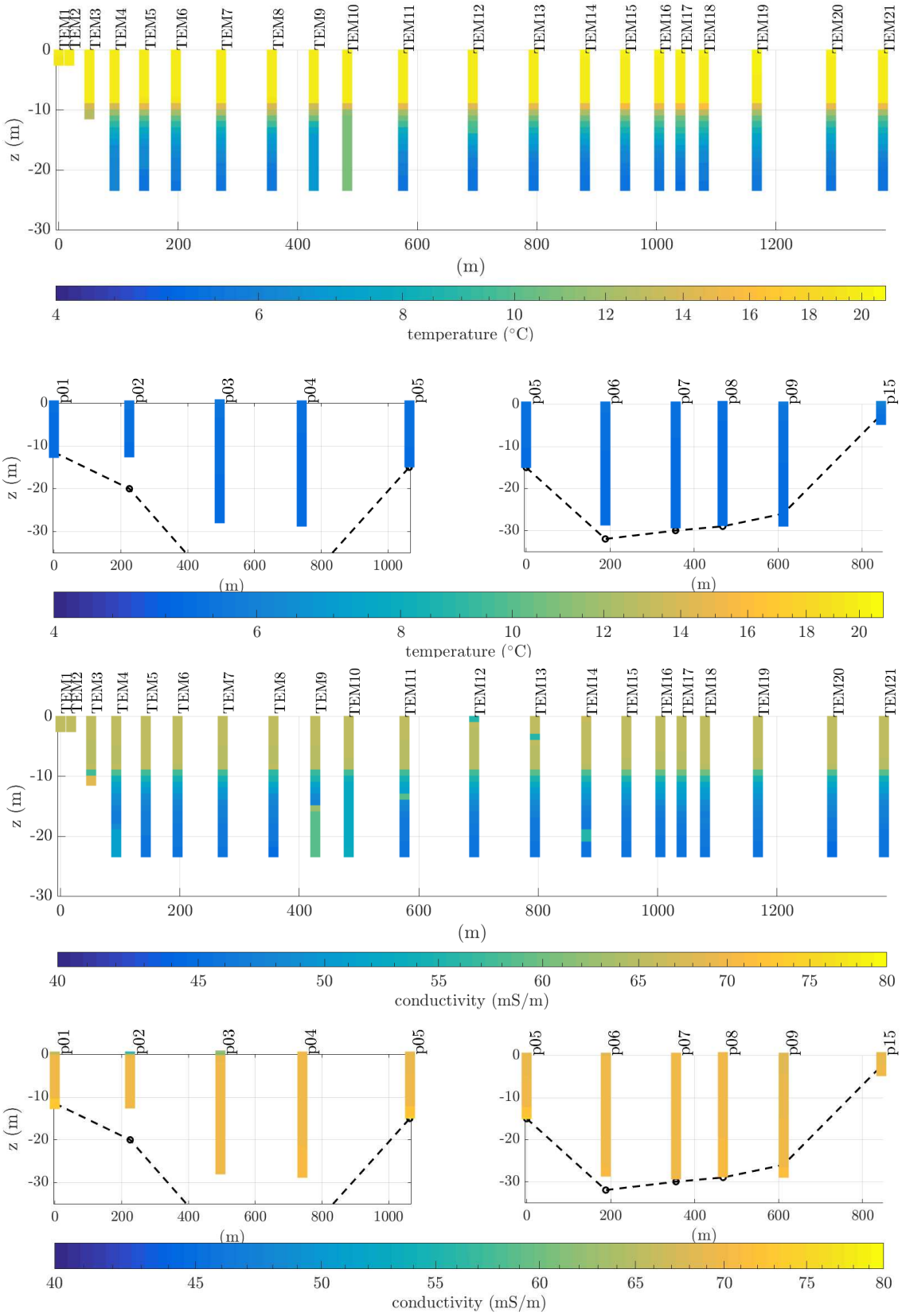

Figure 4.2: Temperature and Conductivity CTD measurement from August 2019 and March 2020.
From top to bottom: Temperature data 2019, temperature data 2020, conductivity data 2019 and conductivity data 2020
The black dotted line indicates the water depth.

4.1.4 Processing and inversion of TEM and ERT data

TEM:

TEM data processing was executed as described in section 3.3.2. Figure 4.3 shows the raw data of the measured signal. The impulse response over time is shown on the left side and the apparent resistivity over time on the right side. All sounding curves decay similarly and without any obvious outliers. Figure 4.4 shows the data after filtering. The measured data was cut to a time interval of $20 - 150\mu s$ to remove datapoints with a low SNR.

As mentioned above, the TEM data from 2019 is not shown, because the device was already damaged during the measurements. Therefore, only TEM data from 2020 is presented on the following pages.

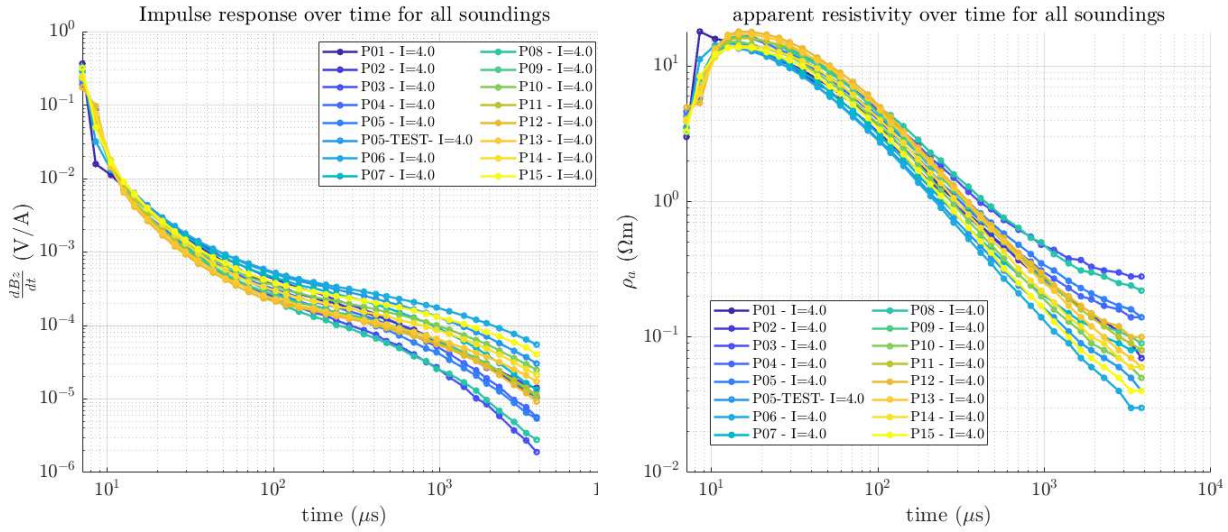

Figure 4.3: Laacher See TEM data from March 2020 - raw data.

After the filtering process, the inversion of the data was conducted by using the parameter values listed in section 3.3.3. The final time spans differed for the individual soundings and different inversion approaches. Table 4.1 shows the time interval for the inversion result, shown in Figure 4.6 on the left side.
For each inversion approach, different start models were created using MATLAB. Laacher See is deeper than the other two measuring sites, which brings a larger water column above the lake floor. Inversion of the data while assuming a single layer to constrain the depth of the water table has proven to be unsuitable for obtaining a model that explains the data sufficiently. Therefore, more layers representing the water depth were generated for the initial models.

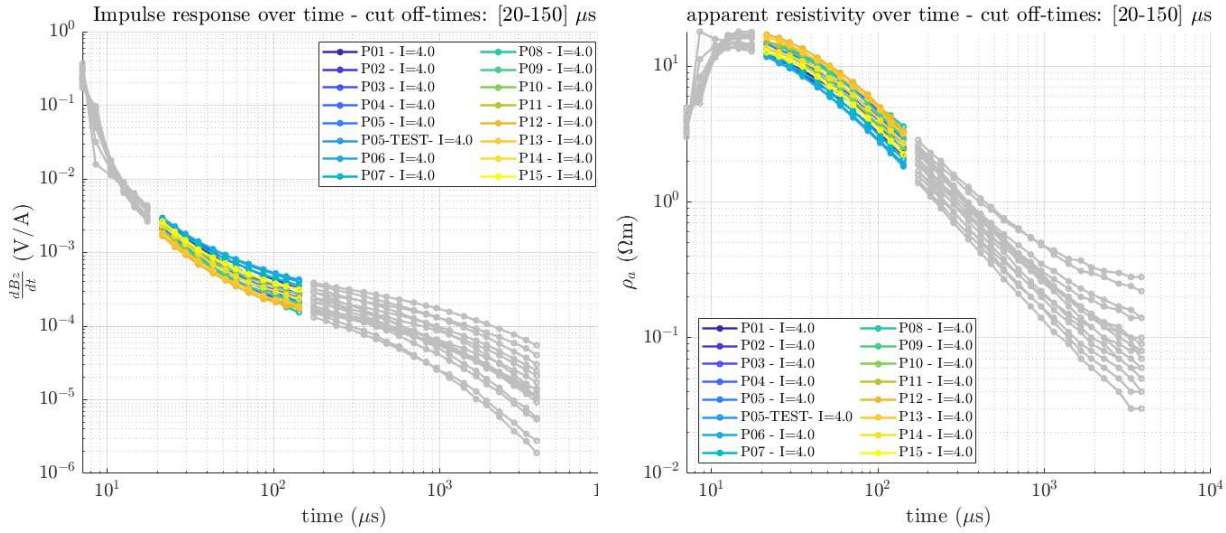

Figure 4.4: Filtering of erroneous data and cutting to low-noise time interval (20-150μs).

sounding-ID	number of datapoints	start time (μs)	end time (μs)
P01	12	21.46	142.3
P02	7	21.46	59.41
P03	7	21.46	59.41
P04	7	21.46	59.41
P05	12	21.46	142.3

Table 4.1: Time interval for each sounding of profile 1 for final inversion approach.

ERT:

ERT data was processed and inverted as described in section 3.3.4.
In Figure 4.5 the ERT data is plotted by visualising the pseudosections of both measuring campaigns.
On the left in Figure 4.5 some sort of error has occurred. This can possibly be traced back to an electrode which was above the water surface. Furthermore, the pseudosection from the measurement in summer (August 2019) shows the expected layering. However, the pseudosection of the ERT data from March 2020 also shows the layering (right plot of Figure 4.5). Because of this observable stratification in the water in the data from winter, it can be assumed that there must be a disturbance here. After checking other ERT profiles, it has been confirmed that all ERT transects collected in March 2020 also reveal the same stratification in the apparent resistivity. Such stratification is not consistent with the homogeneous resistivity values measured in-situ with the CTD probe.

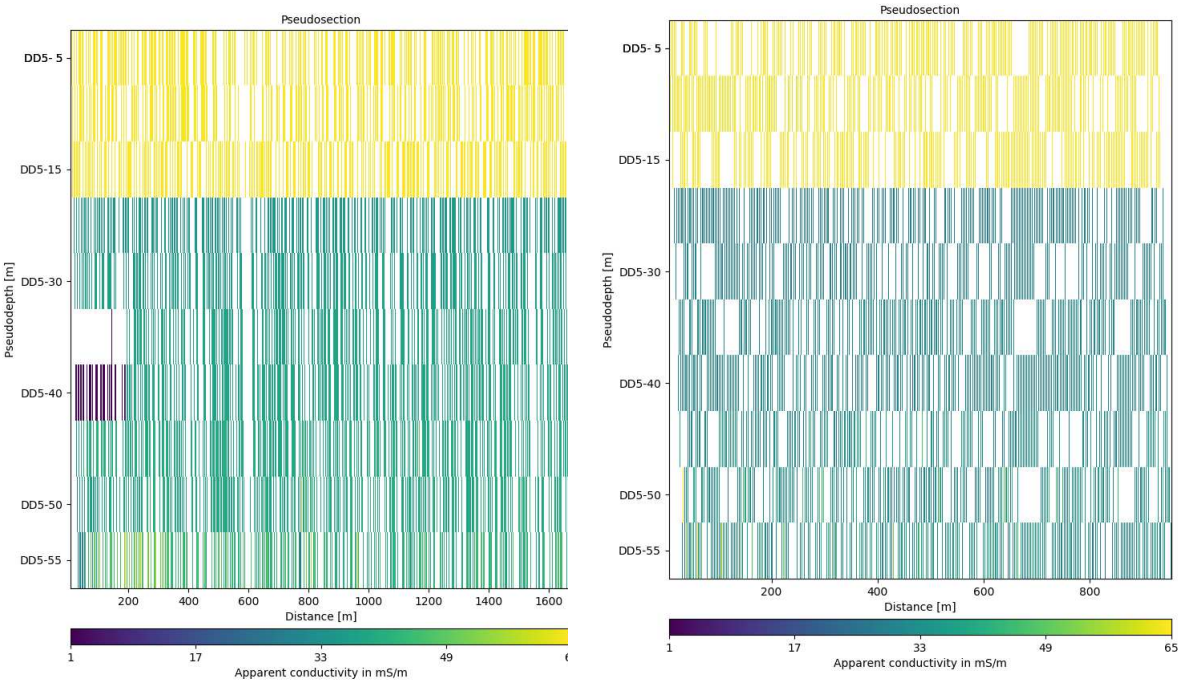

Figure 4.5: Pseudosections of apparent conductivity from August 2019 (left) and March 2020 (right) campaigns at Laacher See.

A possible explanation of this error in the ERT measurements is that the water cable was not floating slightly below the water surface, as it is supposed to, but was towed deep down in the water. For the inversion, the same parameter values were used, as described in section 3.3.4 .

4.1.5 Results and Interpretation

TEM:

Although the data looks smooth in Figure 4.4, it was difficult to get an acceptable fit for the data. The time interval, to which it had to be limited, is narrow compared to the full measuring interval. A comparison of two inversion results is shown in Figure 4.6. This only represents the first profile (P01-P05) as similar results were obtained for the second profile (P05-P15). Figure 4.6 represents two inversion approaches which used different start models, and the CTD conductivity values for the exact same locations to validate the results obtained.

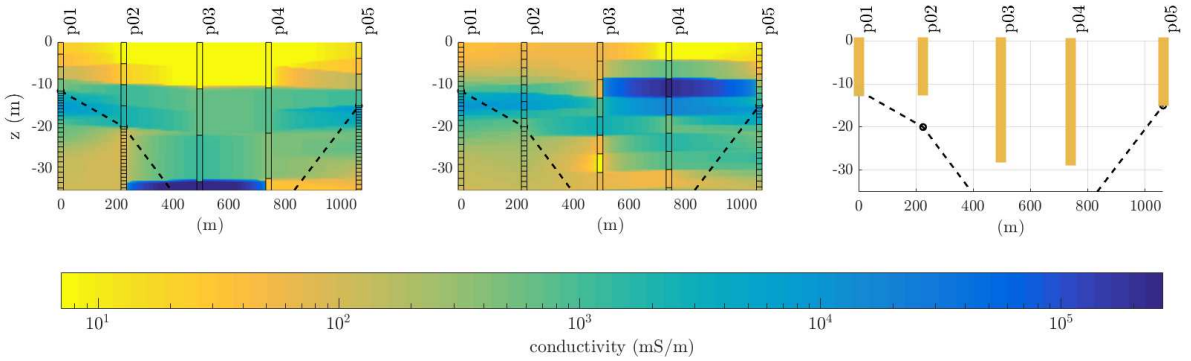

Figure 4.6: TEM inversion models compared to CTP data at the same locations.
In the left subplot a start model with 30 layers was used. The first 4 layers were constrained, using the depth of the water. The four layers have a resistivity value of 70 Ωm and the remaining 26 have a resistivity value of 50 Ωm.
The middle subplot shows the inversion result using a start model with 30 layers. The first 10 layers, representing the water column, were constrained by using the depth of the water. The upper 10 layers have a resistivity of 70 Ωm and the remaining 20 layers have a resistivity of 50 Ωm.
The right subplot shows the CTD conductivity data.

Figure 4.6 shows the comparison of the inversion models of two approaches, which used depth as a constraint. The approaches also used a different number of water layers, and the CTD data of profile 1 are shown as well.
Approaches were performed without constraints and attempts with depth as a constraint, as well as depth and conductivity from the CTD probe as constraints. Figure 4.7 shows an attempt without constraints compared to one with depth as a constraint.

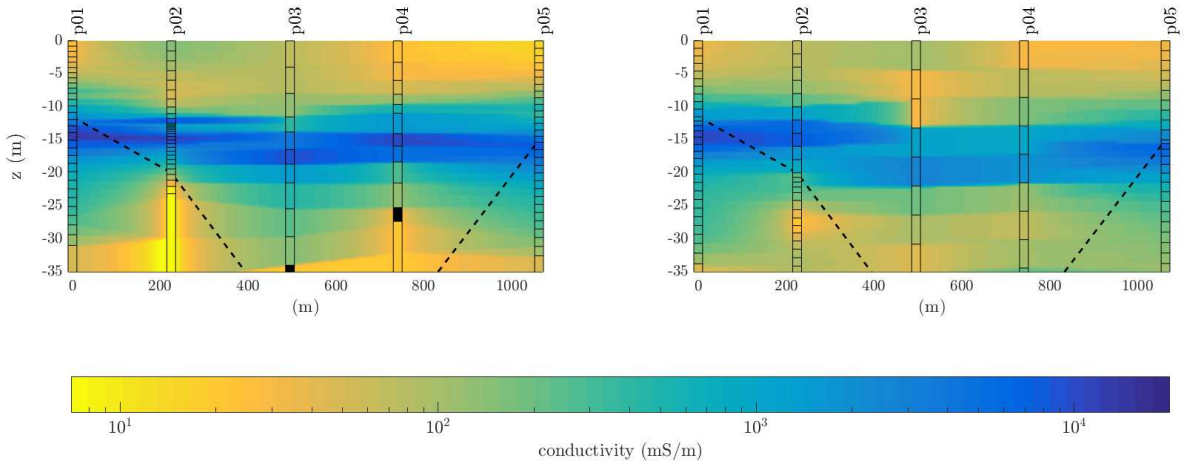

Figure 4.7: Comparison of two different inversion approaches using the same start models and parameter values (standard values from section 3.3.3).
Left side: no constraints; Right side: depth as a constraint.

The same initial model was used for both attempts (30 layers - 10 representing the water column with a resistivity of 20 Ω m and 50 Ω m for the lake subsoil). Furthermore, the

same datapoints were used in both attempts. For approaches with resistivity and depth as a constraint no proper data fit could be achieved.
After comparing several inversion attempts, I observed that all resulting models look alike.

The inversion of the 2020 TEM data resolved a layered water column for all the inversions settings tested here. This is in opposition to the CTD data, which reveal homogeneous values in the electrical conductivity in the water.
The CTD data does not show the layering that is present in the TEM inversion results. According to Aeschbach-Hertig et al. (1996), the layering of Laacher See only occurs in summer. Consequently, a certain disturbance has affected the TEM data, as shown in the unusual layering in the inversion results from March 2020.
Since all inversion models look similar and show the layering of the water, an error resulting from the settings defined for the inversion of the data can be excluded.
A hypothesis for the occurrence of this disturbance is that the metallic boat, pulling the TEM antenna, has been acting as a capacitive source of error for all TEM readings.

ERT:

Another way to validate the TEM results was possible by evaluating the ERT data and comparing the results with the ones from TEM.
Since there are two different effects, causing variations in the TEM and ERT data, the results from both methods from March 2020 cannot be compared meaningfully with one another.
The assumption that the noise in the TEM and ERT data has different sources is confirmed, when looking at the 2020 data. In Figure 4.6 the TEM data shows a resistive layer above a conductive one. On the other hand the pseudosection on the right side in Figure 4.5 shows the opposite - a conductive layer above a more resistive one.
As the ERT data from summer 2019 is correct, a visualization of the inversion result in terms of the resolved electrical conductivity is shown in Figure 4.8 at the top. The above described stratification in the water at Laacher See can clearly be seen in the ERT data. Even when compared with the CTD conductivity data from the same measuring campaign, in Figure 4.8 at the bottom, the model is in good agreement with the CTD data. The thermocline and the chemocline can be seen in a depth of about 10 m in the ERT data as well.

To conclude, it can be stated that there were some malfunctions which affected the data. The observed stratification does not correspond to the values collected with in-situ logs of

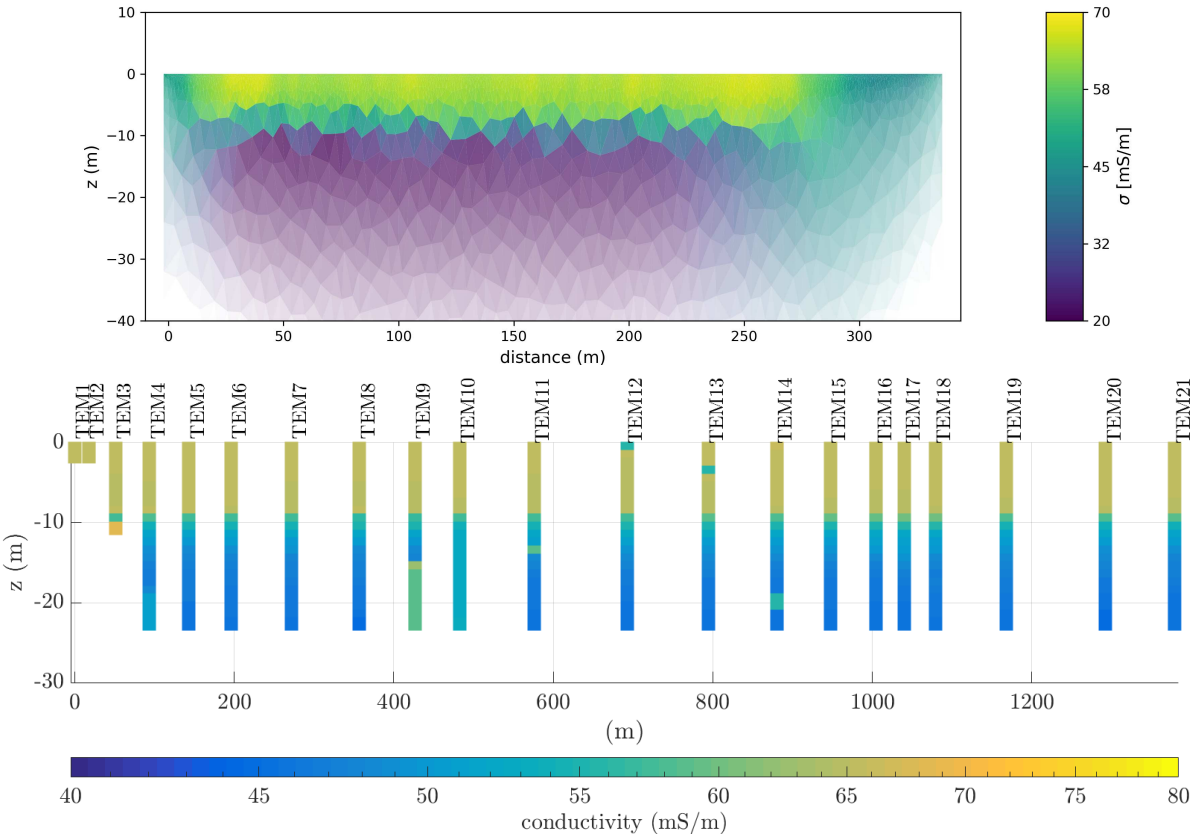

Figure 4.8: ERT inversion result for profile 9 from the measuring campaign in August 2019 and CTD conductivity data from August 2019.

the fluid conductivity and salinity in the lake recorded with the CTD probe. According to Aeschbach-Hertig (1996), the layering of the water only occurs in summer and is therefore not expected to happen in winter. The source of the errors is unknown. The measurement device - the TEM-fast 48 HPC- has been sent in for repairs after the first measuring campaign in August 2019. Two assumptions concerning the error sources have been made. The TEM error effects may originate from the metal boat's influence on the signal. ERT errors may have been caused by the cable sinking deeper into the water instead of floating close to the water surface. When looking at the ERT data from 2019, the mentioned layering of the water can be determined.

To avoid contamination of TEM data it is strongly recommended to use a non-metallic boat to pull the loop and carry the device. ERT measurements can be improved by installing buoys or other objects that will cause the cable to float.

An important conclusion that can be drawn from this case study is that the use of several geophysical methods helps in the interpretation and to detect errors. In case of the Laacher See measuring campaign in March 2020 the CTD probe data did not show the stratification in the lake water that was shown in the TEM and ERT data.

4.2 Case Study 2: Identification of lake sediments in carstic rock (Lake Ocotalito)

4.2.1 Introduction

In this case study TEM data that was measured by Dr. Matthias Bücker was evaluated. The measurements were done to determine and map the thickness of the sedimentary depositions at the bottom of lake Ocotalito. Thus, the objective of the processing is to clarify whether or not these depositions exist in this lake and if TEM can be used to distinguish the sedimentations from the layers above and underneath it.

4.2.2 Study Area

The data was gathered in the summer of 2018 using the 'TEM-fast 48 HPC' (manufactured by AEMR) at lake Ocotalito in Chiapas, Mexico. The lake is located near the city Ocosingo. The evaluated measurement consists of 38 measurements, which were separated into two profiles (see Figure 4.9).

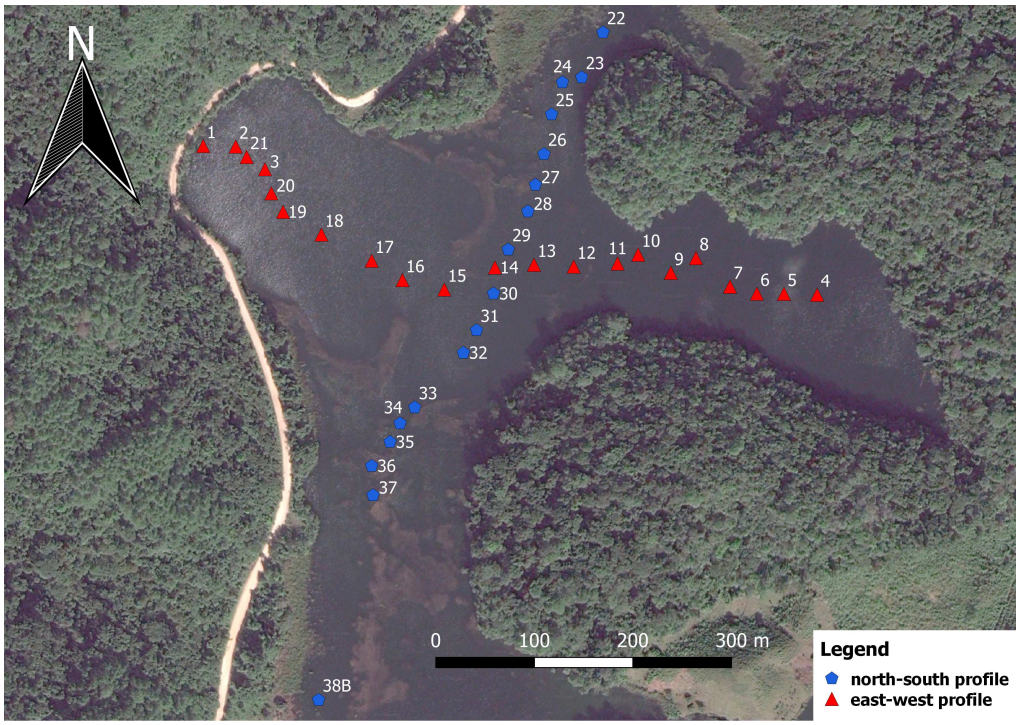

Figure 4.9: Overview of the measuring area at lake Ocotalito.
Soundings 1-21 form the east-west profile (represented by red triangles). Soundings 22- 38b form the north-south profile (represented by blue pentagons).

When looking at a plot of the coordinates, the two profiles are determined by two lines - the first one in east-west and the other one in north-south direction. The TEM loop used had a radius of 11.45 m and an area of about 412 m^2. The data was measured by using 1

Ampere as the transmitter input current. The sampling of the signal was done by using 5 stacks and 32 active time gates with a time interval from 4 - 1024 μs.
From the CTD depth data and additional depth data from Dr. Matthias Bücker an isobath map of Ocotalito was derived, as presented in Figure 4.10.

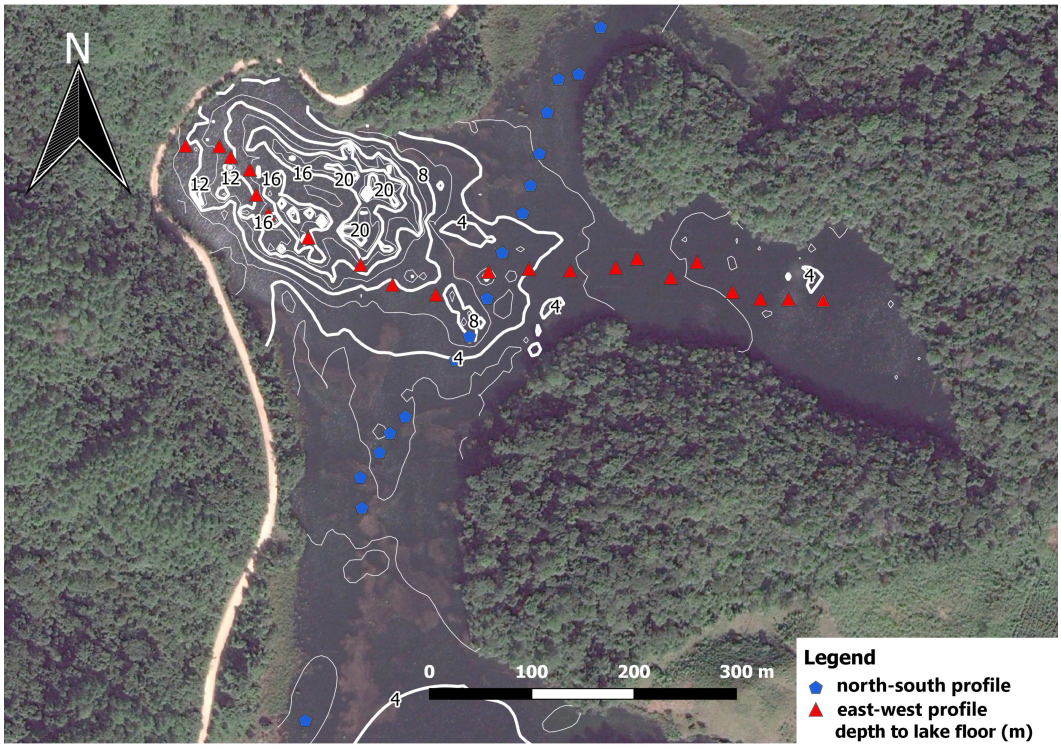

Figure 4.10: Isobath map of Ocotalito derived from interpolation of echo sounder information.

The processing and filtering of the TEM data was executed as described in sections 3.3.2. The visualization of the raw data is shown in Figure 4.11 for the impulse response (left side) and the apparent resistivity (right side). No possible outliers can be seen and the sounding curves decay similarly. The filtering is presented in Figure 4.12, where both, impulse response as well as apparent resistivity are truncated to remove readings with a low SNR. The remaining low noise interval is 20 - 110 μs. Figures 4.11 and 4.12 are shown exemplary for the north-south profile.

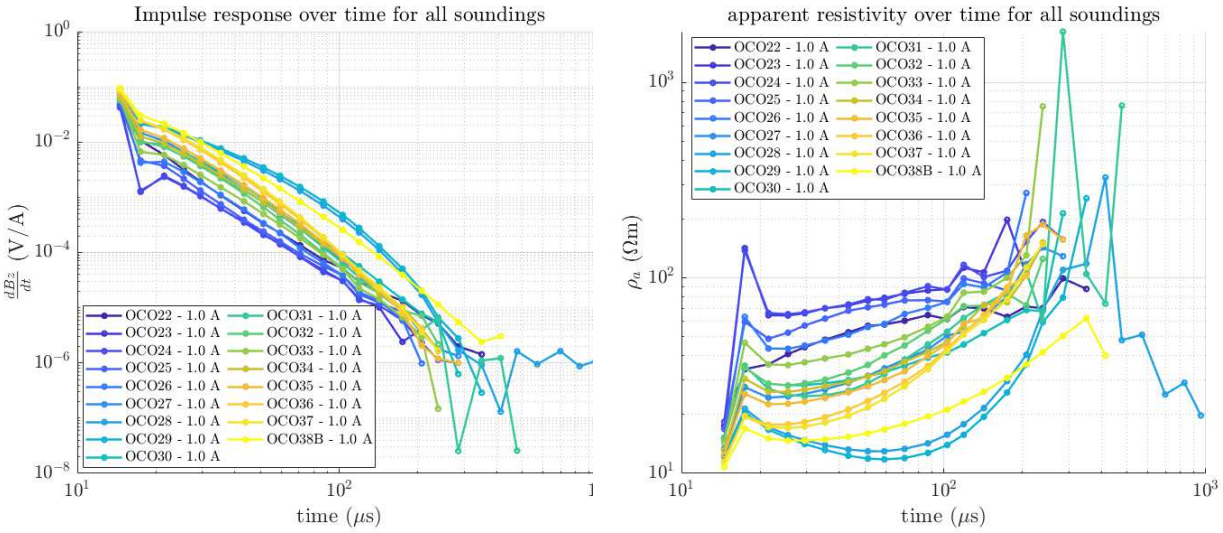

Figure 4.11: Ocotalito north-south profile - raw data visualization.

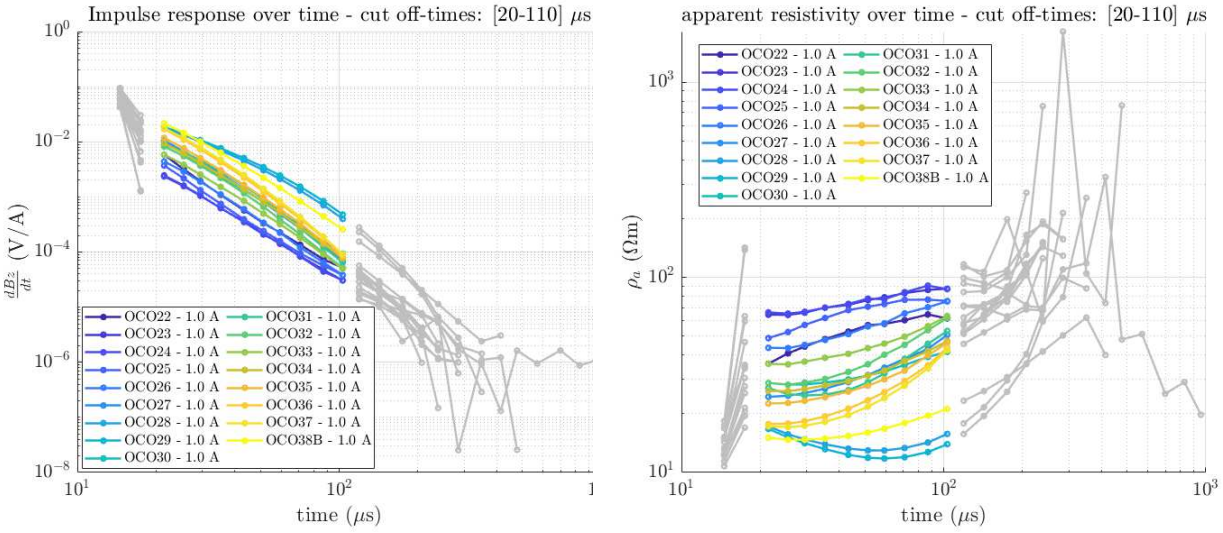

Figure 4.12: Ocotalito north-south profile - filtering of erroneous data and cutting to low-noise time interval (20-110μs).

After the filtering, the inversion process was conducted as described in section 3.3.3. The same inversion parameter values, as described in section 3.3.3 were used. Only the style option (*smooth*, *standard* and *focused*) differed, depending on the respective inversion approach. The goal of the inversion process was to obtain a 1d-multi-layer model for each separate-sounding. These 1d-models were interpolated using MATLAB to obtain a 2d model of the subsurface (Figures 4.15 - 4.17). The start models for the soundings were created with MATLAB. The maximum depth of the start model was chosen to be 35 m. For some approaches the bathymetric information, measured by an echo sounder, and the resistivity of the water were used as constraints in the inversion. The thickness of the first layer was fixed to the value which was gained through the echo sounder. When resistivity was used as a constraint, a mean value for the first layers of all soundings was calculated after a first test inversion. This resulted in 20 Ωm for the mean value. No complementary geophysical data was available to evaluate the obtained results. Therefore, three inversion models were compared to see how the results change with different settings and start models.
The inversion approaches differed in the amount of layers of the start model, which parameters got constraint, and the style option that can be chosen in ZondTEM1d.
The three inversion approaches discussed on the following pages are:

- smooth inversion without constraints (30 layer start model with 100 Ωm for all layers)
- smooth inversion with bathymetry and mean of water resistivity as a constraint (30 layers - first layer: 20 Ωm and 100 Ωm for the remaining layers)
- standard inversion with bathymetry as a constraint (15 layers - first layer: 20 Ωm and 100 Ωm for the remaining layers)

Table 4.2 shows the final time intervals used for each sounding of the NS-profile for the no constraints approach.

sounding-ID	number of datapoints	start time (μs)	end time (μs)
oco22	9	21.46	87.07
oco23	8	25.49	87.07
oco24	8	25.49	87.07
oco25	10	21.46	103.2
oco26	9	25.49	103.2
oco27	10	21.46	103.2
oco28	10	21.46	103.2
oco29	9	21.46	87.07
oco30	10	21.46	103.2
oco31	6	25.49	59.41
oco32	7	25.49	70.95
oco33	10	21.46	103.2
oco34	10	21.46	103.2
oco35	8	21.46	70.95
oco36	8	25.49	87.07
oco37	6	25.49	59.41
oco38B	10	21.46	103.2

Table 4.2: Time interval for each sounding of north-south-profile at Ocotalito. These values represent the inversion approach without constraints.

4.2.3 Results and Interpretation

Figure 4.13 shows the filtered data used for the inversion for the no-constraints approach on the right side. The left side shows the corresponding inversion models. Only one example is shown, because the models resulting from the different inversion approaches look similar. A linear interpolation of the inversion models for all the soundings was done to get a 2D model of the subsurface, as represented in Figures 4.14, 4.15, 4.16 and 4.17.

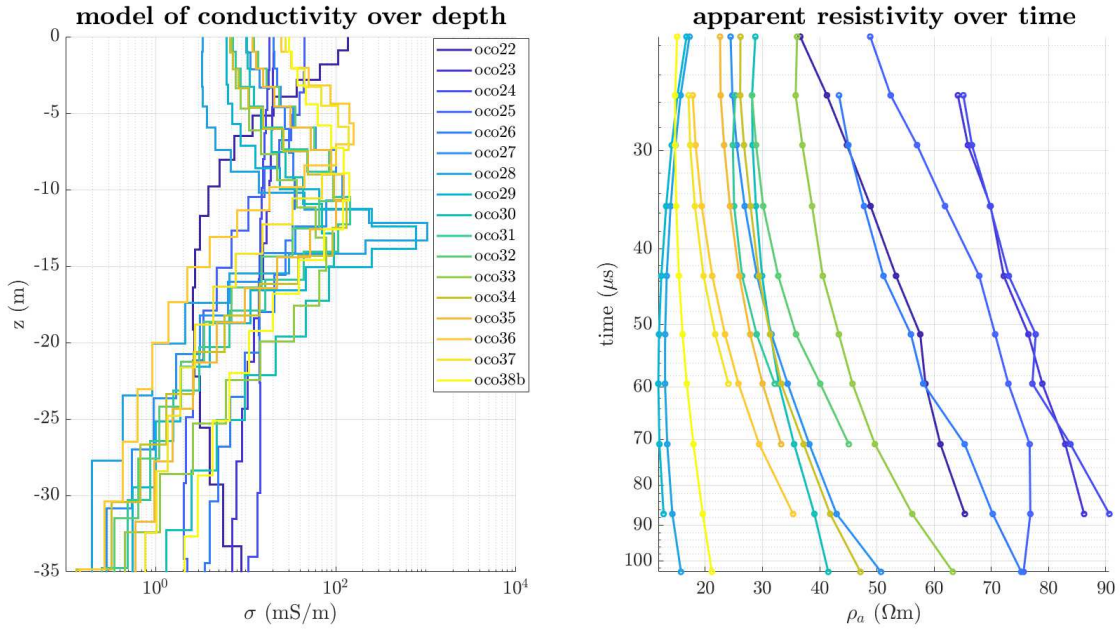

Figure 4.13: Left graph: Depth model of conductivity resulting from inversion of TEM data for a **non constraint approach**.
Right graph: The corresponding apparent resistivity information - the remaining datapoints used for the calculation of the inversion model for each sounding.

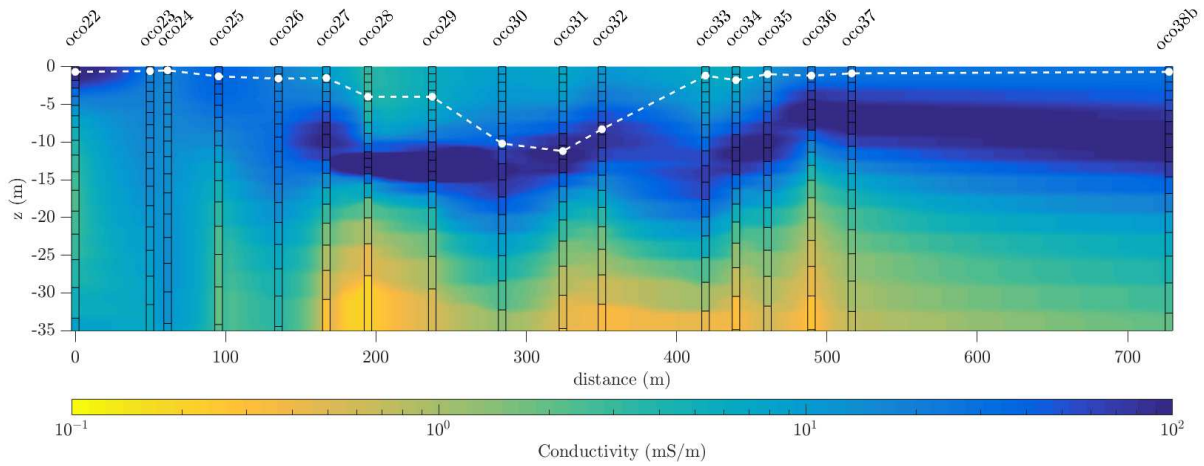

Figure 4.14: Linearly interpolated inversion model for the style option **smooth** with a **30 layer starting model** and **no constraints** for the **north-south profile**. The black squares represent the TEM log of each sounding. The white dotted line marks the water depth, which was measured by an echo sounder. It was linearly interpolated between the points.

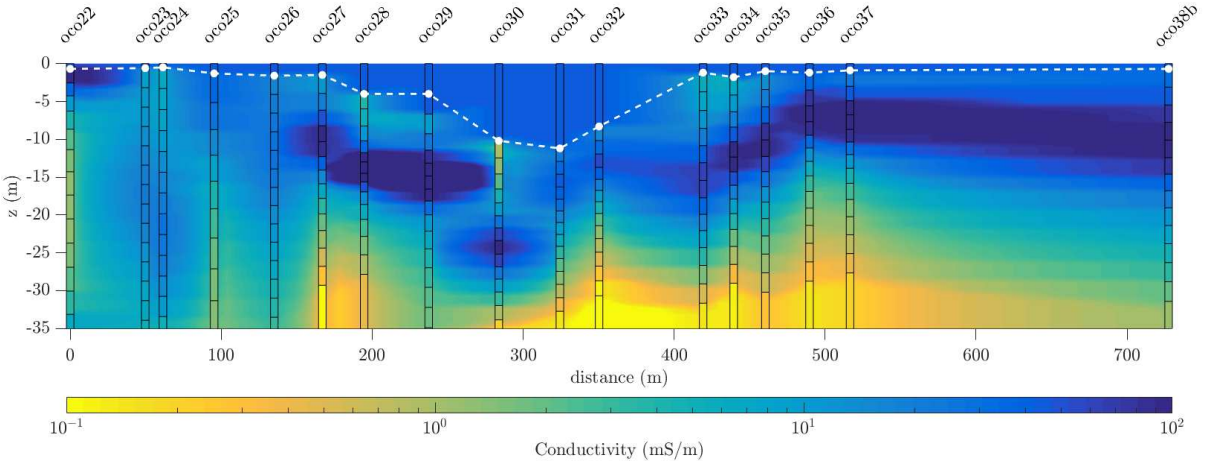

Figure 4.15: Linearly interpolated inversion model for the style option **smooth** with a **30 layer starting model** and **depth and resistivity as constraints** for the **north-south profile**. The black squares represent the TEM log of each sounding. The white dotted line marks the water depth.

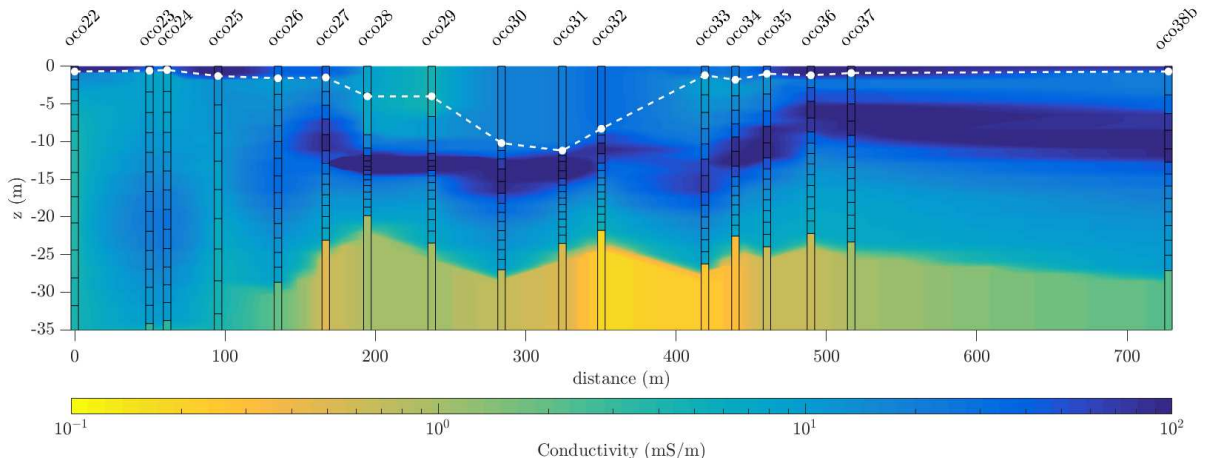

Figure 4.16: Linearly interpolated inversion model for the style option **standard** with a **15 layer starting model** and **depth as a constraint** for the **north-south profile**. The black squares represent the TEM log of each sounding. The white dotted line marks the water depth.

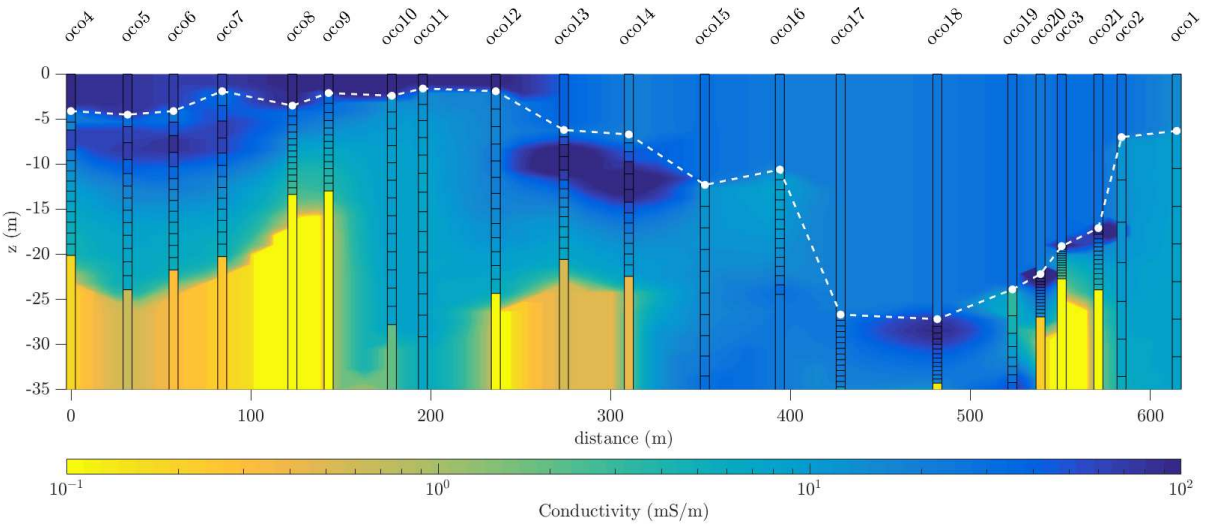

Figure 4.17: Linearly interpolated inversion model for the style option **standard** with a **15 layer starting model** and **depth as a constraint** for the **east-west profile**. The black squares represent the TEM log of each sounding. The white dotted line marks the water depth.

Figures 4.14 and 4.15 show the inversion results with and without constraints, respectively. Not many differences can be seen when comparing the two figures, even though Figure 4.15 used additional information for the inversion. Figure 4.16 also looks similar, when compared to Figures 4.14 and 4.15. In contrast to Bücker et al. (2020), an improvement of the imaging results cannot be seen when constraining the resistivity of the water layer. According to the results, the sediments are present only in some areas of the lake. The bedrock layer follows the bathymetry - it is deepest, where the water depth reaches its maximum.

In Figure 4.15 a high resistive anomaly can be seen at sounding 'oco30'. This could either indicate accumulated rocks (which is less likely, due to the fact that no other inversion result shows this anomaly) or an artefact coming from the change of resistivity from water to the layer underneath.

In the results of the three different inversion approaches for the north-south profile, four layers are visible from 200 m until the end. The water layer can be seen on the top, with a rather resistive sedimentary layer underneath it. This layer is followed by a more conductive layer, which may correspond to higher saturation, bigger pores or an increase of clay content. At the bottom the bedrock can be seen, which is probably limestone, according to the conductivity values.
In contrary to the expectations a sedimentary layer cannot be seen in most of the shallow parts of the profiles e.g. in the north-south profile between 0 and 350 m (shown in Figures 4.14 - 4.16). The sediment layer cannot be seen in the east-west profile between 120 and 240 m (shown in Figure 4.17). The lack of sediments in some parts of the lake could result from the shallow depths in most areas of the lake, where the depth does not exceed 4 m (shown in Figure 4.10). Bücker et al. (2020) also assumed that in shallow water depths the bedrock is not covered by conductive sediments, which may also be the case in this field study.

Comparing the results from the different inversion approaches (Figures 4.14 - 4.16), a geological model for the north-south profile was derived, as shown in Figure 4.18. This geological model shows the four above described layers. The sedimentary deposits only seem to occur from 350-700 m in the north-south profile.

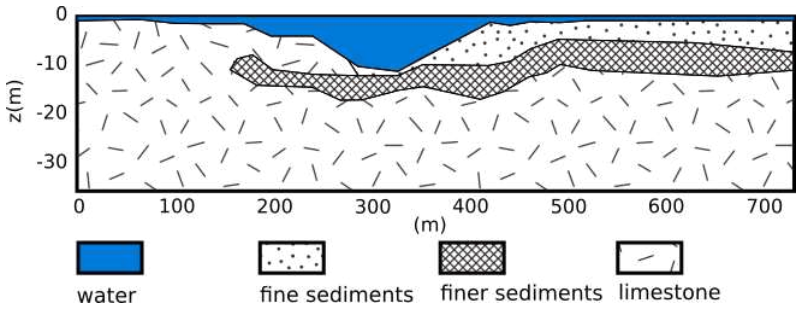

Figure 4.18: Derived geological model for the north-south profile.

Figure (4.19) illustrates the datafit of two different soundings. The datafit provides information on how good the calculated inversion model represents the measured data. For some measurements less datapoints had to be removed (oco27) than for others (oco31), to get an acceptable datafit, as presented in Figure 4.19. For noisy sounding-curves more points were removed to get a smoother curve that can be fitted more easily.

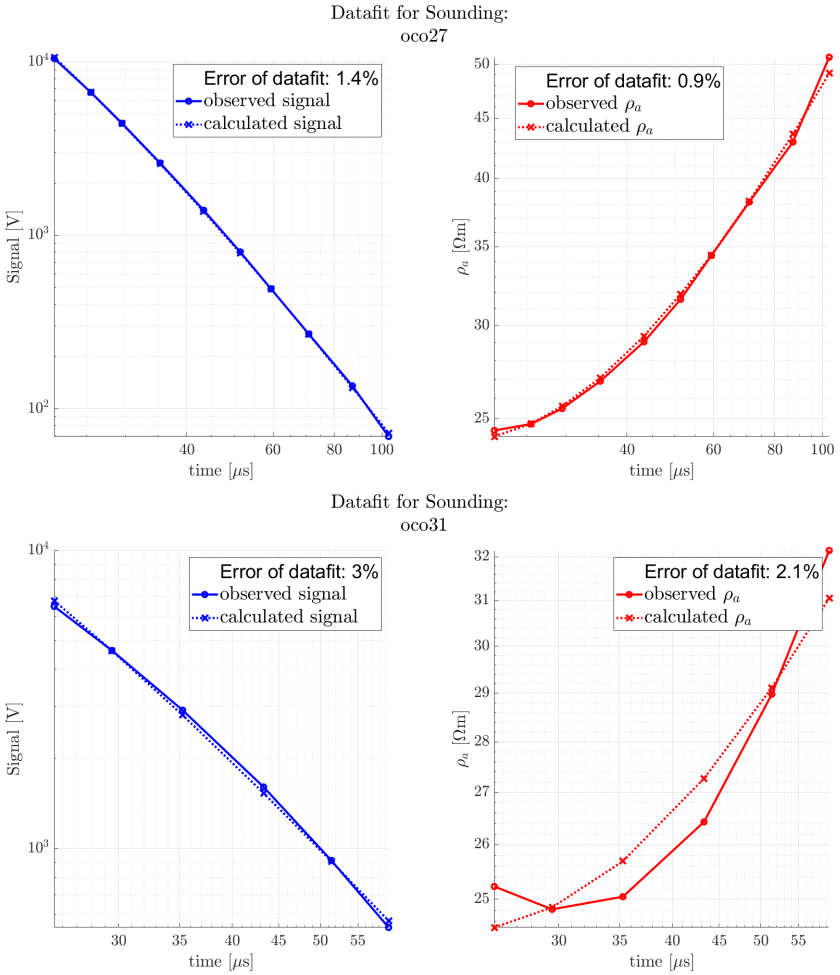

Figure 4.19: Datafit for soundings oco27 and oco31.
oco27 contains all points from the first filtering (corresponds to ten), whereas oco31 holds only six datapoints.

Three homogeneous start models with 30 layers and different resistivity levels (5, 50 and 150 Ωm) were created and inversions were carried out, to check whether the obtained inversion model depends on the data or the start model. The inversion parameters and the settings from the inversion that produced the best result, were used for random soundings along the profiles. To not go beyond the scope of this thesis, results are presented only for one sounding in Figure 4.20.

From this Figure it can be concluded that the inversion model can be trusted until a depth of about 40 m. At this depth the different models change their curse depending on the resistivity value used in the initial model.

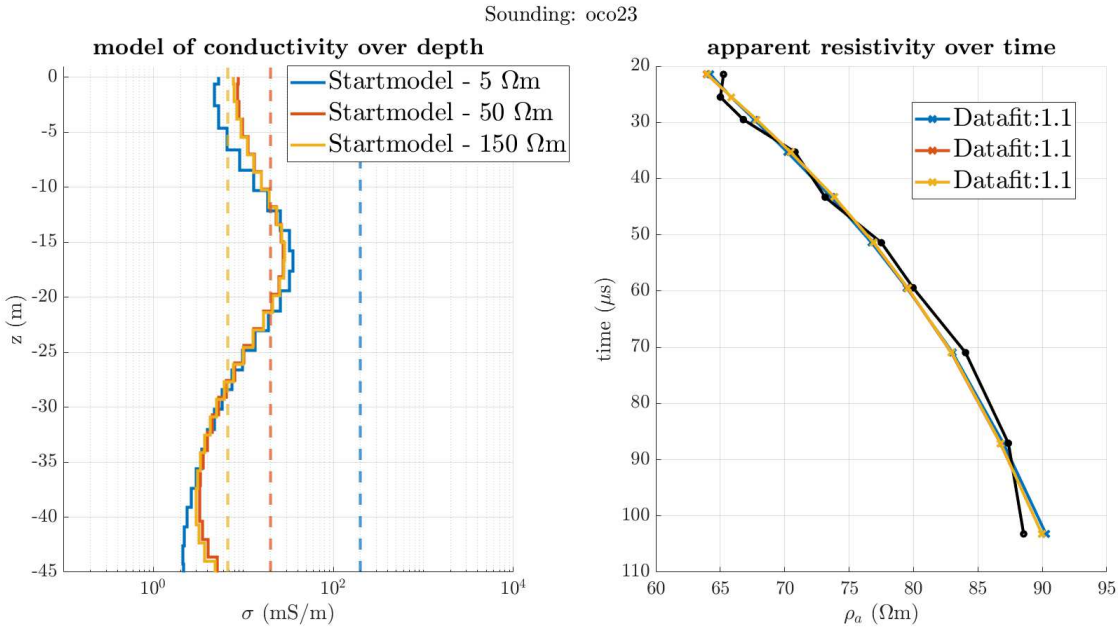

Figure 4.20: Inversion results using three different homogeneous start models with 30 layers and three different resistivity values. Exemplary for TEM sounding 'Oco23'. Left side: inversion models. Right side: data points used for inversion and datafit for the three approaches.

To sum up, the different inversion approaches do not significantly change the result of the inversion model. The choice of inversion style option only has a small impact on the result. In some areas of the Ocotalito lake it is difficult to determine the sedimentary deposits. There are two options why that is the case, either the resolution of the TEM-device was too low to detect thinner sediment layers or there is no sedimentary deposit above the bedrock in some areas. In the southern region of the north-south profile there may be a sedimentary layer, which has an extent of a few meters. However, the same conclusion can be reached as in the case study before:

Without supplementary information, e.g. about the water flow in the lake, borehole information or data from complementary geophysical methods, no secured statement about the thickness and occurrence of the sedimentary layer can be made. As no complementary

geophysical data was available, the interpretation of the inversion results from this thesis needs to be treated with caution.
Consequently, verifying measurements with various geophysical methods will improve the interpretation.

4.3 Case Study 3: Identification of lake sediments in a former opencast mining site (Bergwerksee Langau)

4.3.1 Introduction

The measuring campaign on Bergwerksee near Langau aimed at investigating whether TEM can resolve the sedimentary layer underneath the lake water and to characterize the geometry of the same. Furthermore, it should also be determined, if additional a-priori information from complementary methods has a positive influence on the TEM-inversion result. From the last chapter it can be concluded that an interpretation of the inversion results from TEM-data is challenging without information from complementary methods. Furthermore, it becomes difficult to verify the resulting model without additional information. Therefore, complementary data, collected with a CTD-probe, was included in the inversion process. From the CTD data, resistivity and depth of the water layer can be either used as a-priori information for a constraint inversion or for a more accurate start model.
ERT-measurements were also conducted for validation of the TEM-inversion results.

4.3.2 Study area

The measuring area, called Bergwerksee, is situated in Lower Austria, near the town Langau, in the district of Horn. The lake used to be an opencast coal mine, which was flooded by directing the nearby creek into the opencast mine, as the profits decreased due to the lacking quality of the coal.

During a two day measuring campaign on the 27th & 28th of May 2020, 11 ERT profiles and 39 TEM-soundings with CTD-probe measurements at the same locations were conducted, shown in Figure 4.21. The used instruments were the 'TEM-fast 48 HPC' (by AEMR), the 'Syscal Pro Switch 72' (by IRIS Instruments) and the 'Aqua Troll 200 Data Logger' (by In-Situ) for TEM, ERT and CTD-measurements.

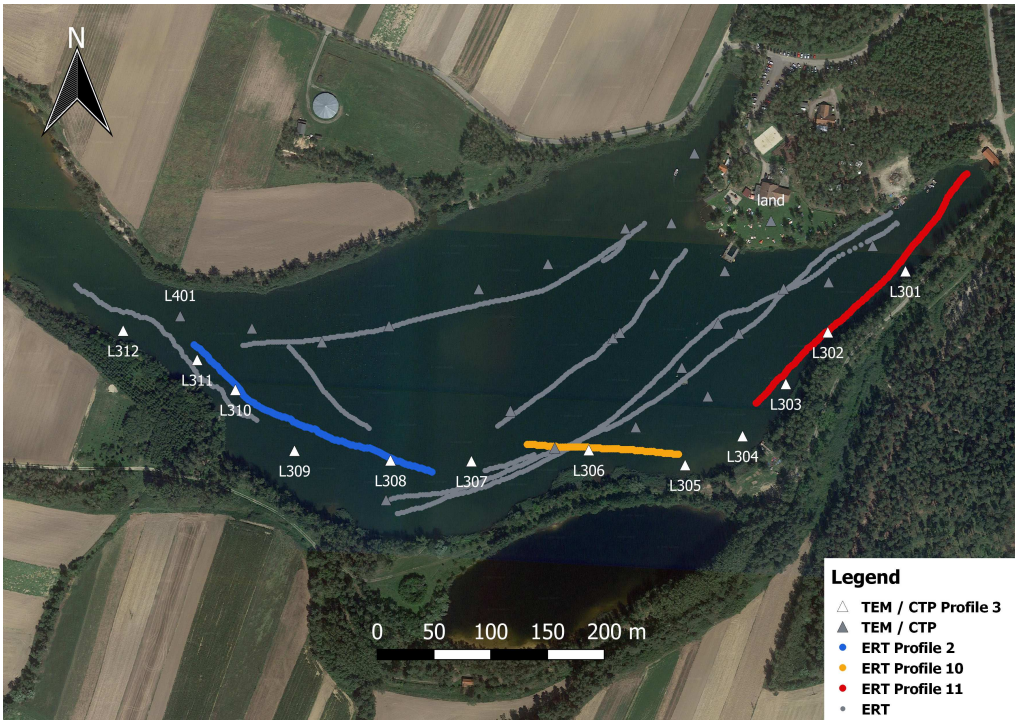

Figure 4.21: Overview of the measuring area at Langau from late May 2020. TEM, ERT and CTD measurements were conducted over the time of two days. A continuous CTD measurement was done at every TEM-sounding location.

The same configuration for the loop, as described in the first case study at Laacher See - a 45 m carrier loop with a 50 m cable attached to it, was used for TEM measurements. The TEM antenna has a radius of 7.2 m and an area of 161 m^2.
4 Ampere were used as transmitter current with 3 stacks. For the sampling of the signal, 36 active time gates between 4 - 2048 μs were set. While measuring, the loop was separated from the boat by 2.5 m.

The ERT data was measured by using the water cable described in section 2.2. A dipole-dipole configuration was used, where the last two electrodes, namely the ones farthest from the boat, were the current dipole.

4.3.3 CTD data

At every TEM sounding a CTD measurement was done, after having finished with the TEM measurement. Figure 4.22 represents the CTD conductivity and temperature data. The conductivity and temperature data are consistent along the profile.
Figure 4.23 shows an interpolation of the depth measured along the lake with the CTD probe.

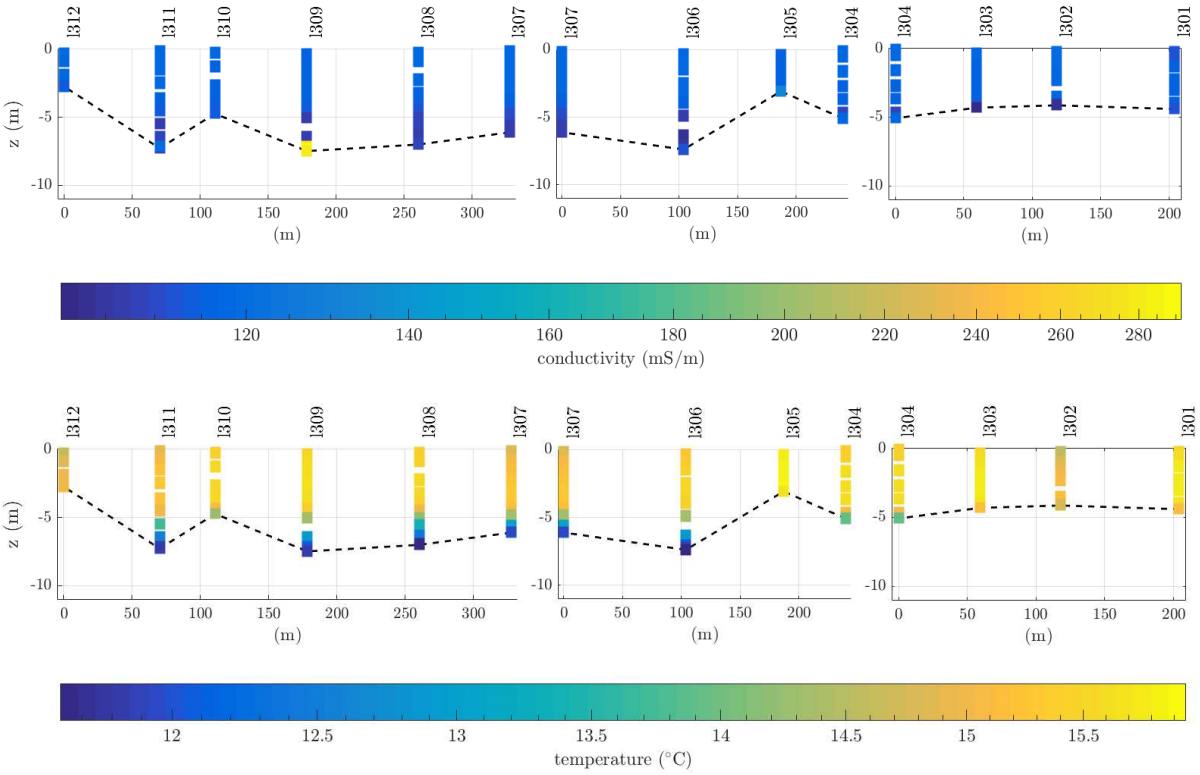

Figure 4.22: Conductivity and temperature CTD measurements for each TEM location of profile 3.

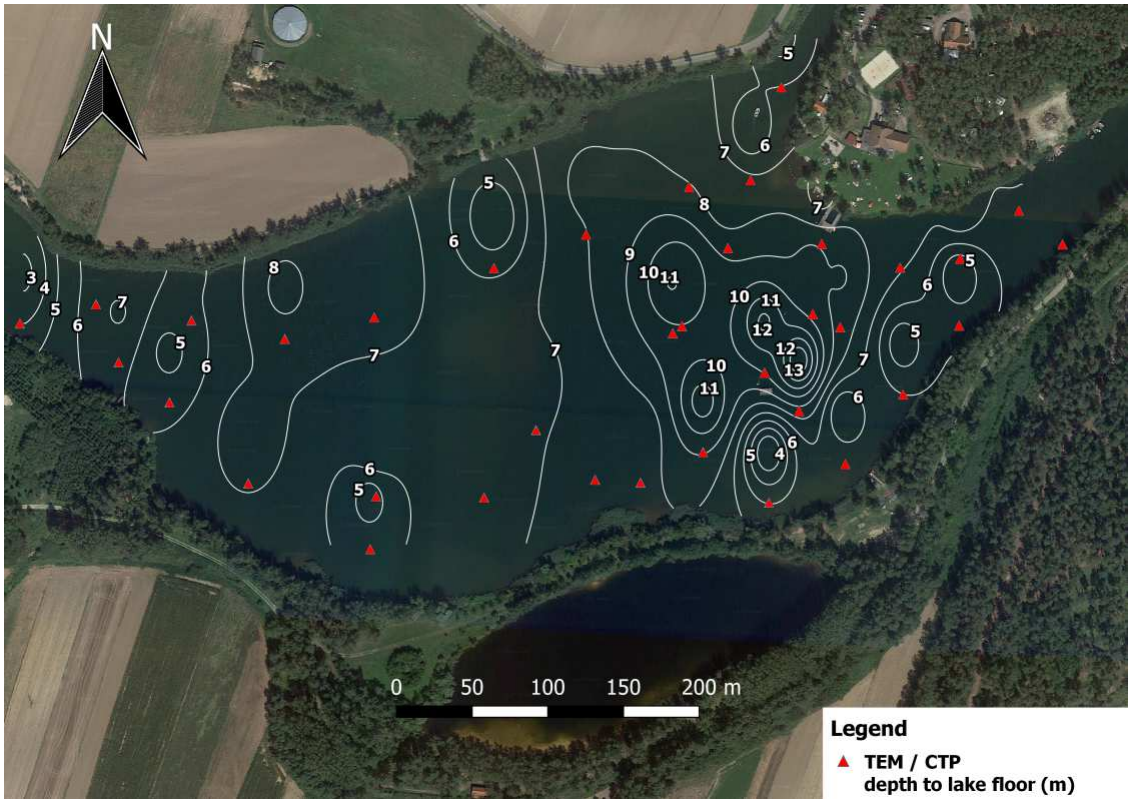

Figure 4.23: Isobath map of Bergwerksee using the depth information from the CTD probe.

4.3.4 Processing and inversion of TEM and ERT data

A selection of TEM measurements, which form Profile 3 (shown as white triangles in Figure 4.21), was evaluated. Three ERT profiles (blue, orange and red lines in Figure 4.21) were inverted and compared to the TEM inversion models for validation reasons. The processing and filtering of the TEM data was executed as described in section 3.3.2. Figure 4.24 shows the measured raw data, which look similar for all sounding curves and Figure 4.25 shows the filtered data. The soundings were truncated to a time interval of 8-120 μs to cut out readings with a low SNR.

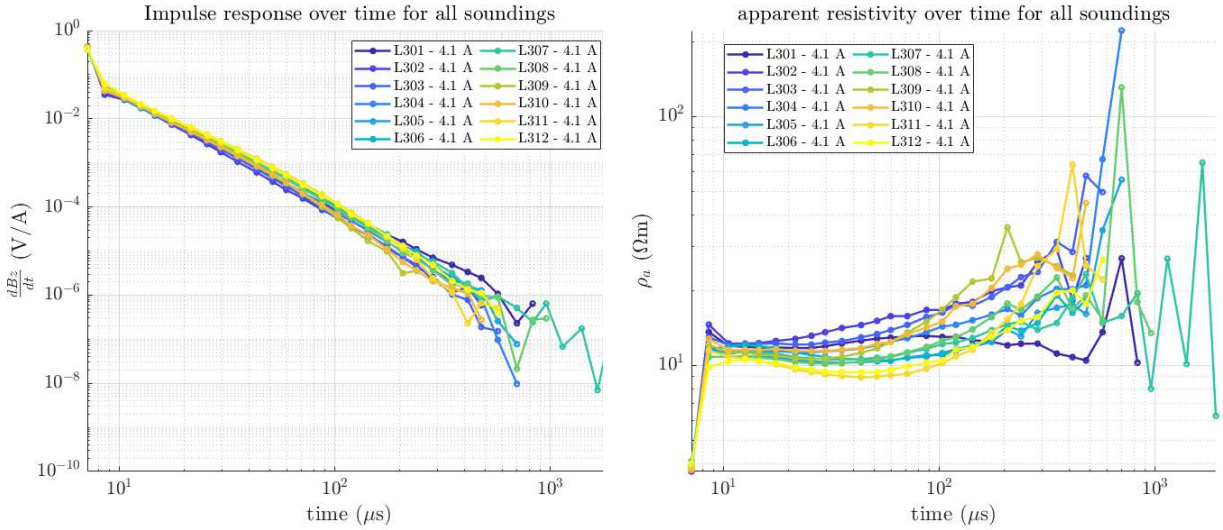

Figure 4.24: Raw data visualization for profile 3

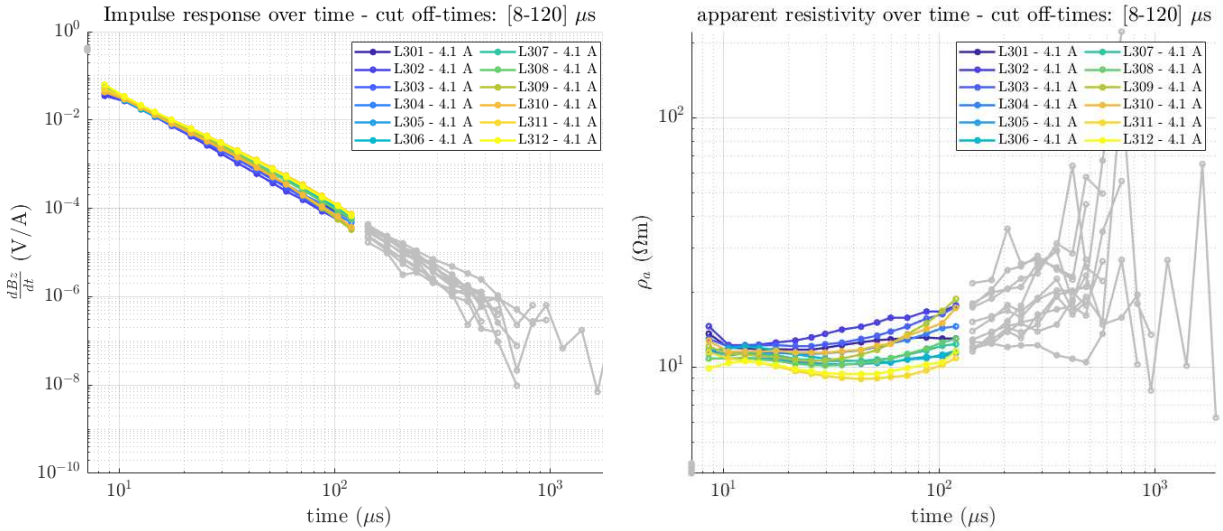

Figure 4.25: Filtering of erroneous data and cutting to low-noise time interval (8-120μs) for profile 3.

After the filtering the inversion process was executed as described in section 3.3.3, using the 'standard' inversion parameter described in the same section.

The water depth and the resistivity data, measured with the CTD-probe, were used to form a more accurate start-model and as constraints in the inversion process.

After test inversions, it was clear that constraining the resistivity information has no significant impact on the resulting model. Figure 4.28 shows a comparison between the conductivity values of CTD and TEM in the water layer. This example represents an inversion approach where the resistivity of the water is not constrained. The CTD conductivity and the inverted conductivity model show a good accordance. Therefore, only the depth information by the CTD data was used as a constraint in the inversion process.

The final inversion approach uses a start model consisting of 30 layers. The first layer was constrained, using the depth measured by the CTD probe. The resistivity for this first layer was set to 10 Ωm, which is the mean value of the CTD resistivity measurements. 50 Ωm were set for the remaining 29 layers. The maximum depth of the start model was 40 m.
Table 4.3 shows the final time spans used for the inversion for each sounding of profile 3.

sounding-ID	number of datapoints	start time (μs)	end time (μs)
L301	15	10.53	119.2
L302	15	10.53	119.2
L303	16	8.52	119.2
L304	16	8.52	119.2
L305	14	12.55	119.2
L306	15	10.53	119.2
L307	16	8.52	119.2
L308	16	8.52	119.2
L309	11	10.53	59.41
L310	14	10.53	103.2
L311	16	8.52	119.2
L312	15	8.52	103.2

Table 4.3: Time interval for each sounding of profile 3 for the final inversion approach.

4.3.5 Results and interpretation

Figure 4.26 shows the final inversion model.

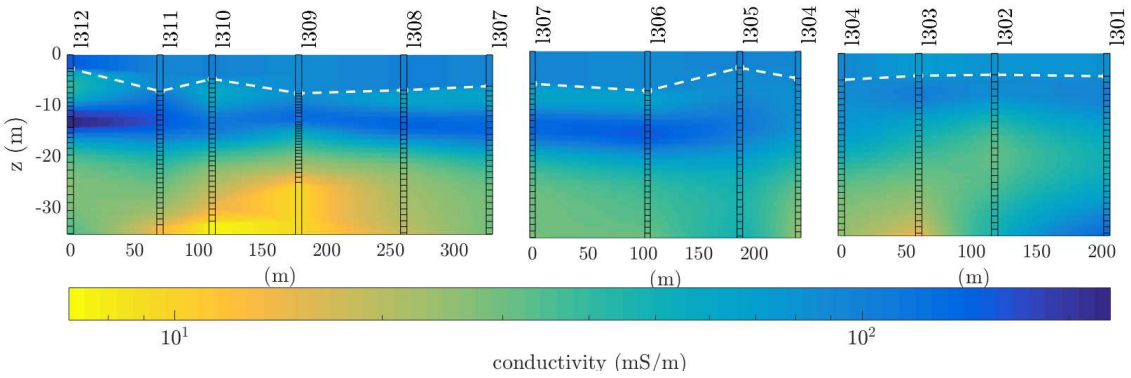

Figure 4.26: Interpolation of the final inversion model. Black rectangles show the TEM sounding locations. The white line indicates the water depth. The name of each sounding is plotted above its location. The distance on the x-axis is measured from the first sounding in each line.

The contrast in the colors, presented in Figure 4.26, can be interpreted as different lithological layers - in this case the inversion result can be described by four layers:

- The top layer is the water column. It is delimited by the white line (water depth). It has a conductivity of approximately 90 mS/m
- The second layer shows the sedimentary layer with a lower conductivity compared to the top layer. It can be seen that it is bigger where the lake is deeper (l309 - l306). This is explained by currents that may have transported the sediments there.
- The third layer shows a higher conductivity than the sediment layer and starts at a depth of about 10 m. This layer seems to contain finer sediments compared to the layer above. It might be the area with the highest clay content in this section.
- The bottom layer shows the lowest conductivity values of all in this subsurface zone, which can be attributed to less clay occurrence or (as well) more coarse sediments.

An increase in the electrical conductivity can be seen between the assumed sediment layer and the layer underneath it. This can attributed to Archies Law (1.4). This formula shows that the electrical conductivity increase can be either a consequence of different saturations of the materials or a difference in porosity. Assuming that the substances are fully saturated because of the lake above them, the rise in conductivity is explained by a change in porosity.
Figure 4.27 shows a geological model for the subsurface section. It was derived using the interpretation of the results.

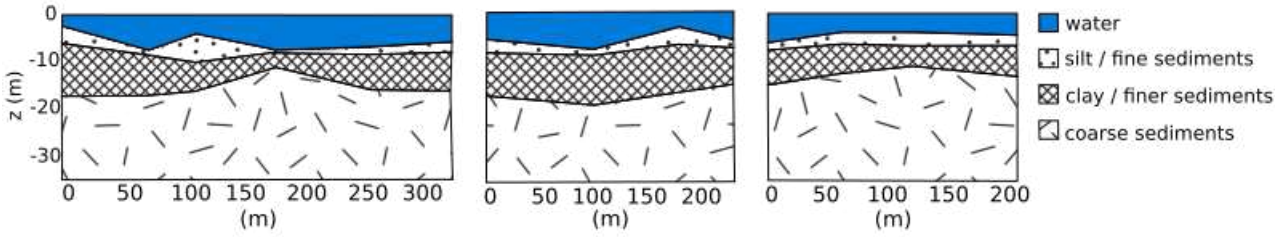

Figure 4.27: Assumed geological model for profile 3.

Two verifications were carried out, to evaluate whether the final inversion approach has good credibility.
Figure 4.28 shows the agreement of the CTD resistivity data with the inversion model.

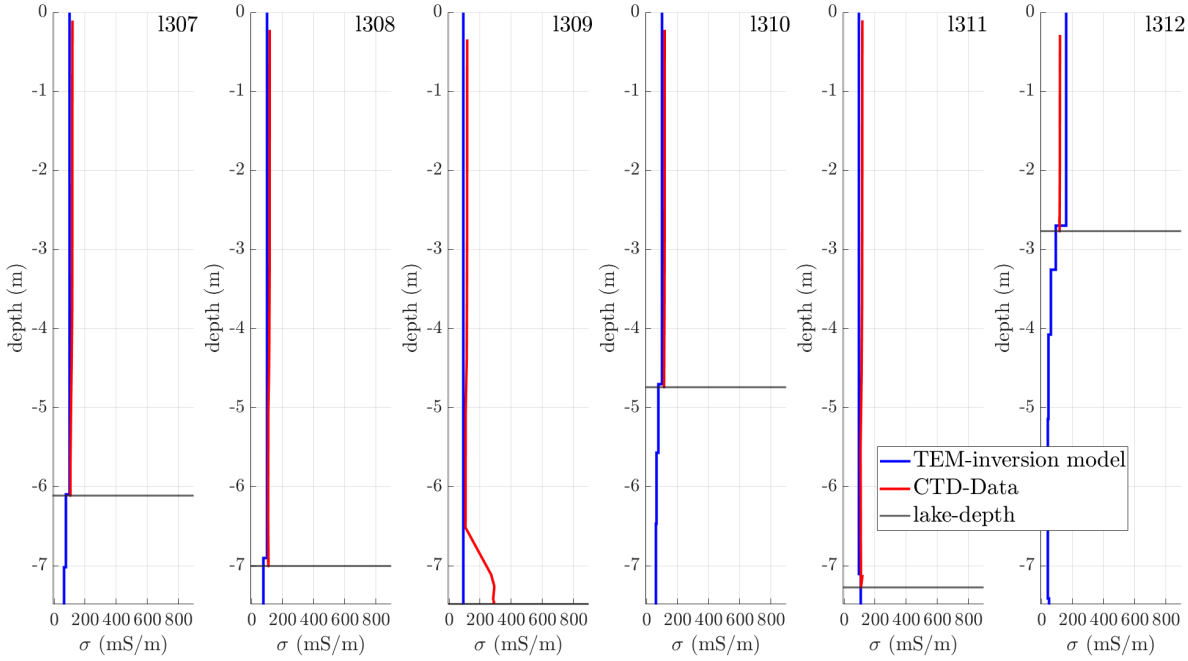

Figure 4.28: Comparison of TEM and CTD conductivity. Exemplary for a part of TEM profile 3.

The conductivity values of TEM and the CTD probe are conform. This means that the inversion shows good results for the water layer. Therefore, it is not necessary to use the CTD resistivity as a constraint in the inversion process.

Another verification was done to find out until which depth one can possibly trust the resulting inversion model. It was determined whether the inversion is dominated by the data or by the starting model. For this purpose three different homogeneous start models were used with one and the same inversion parameters from the inversions before. The

three start models differed from each other only by the resistivity value. The chosen values were 7, 50 and 170 Ωm.
This evaluation was done for three random soundings of profile 3. Figure 4.29 displays the results for 'L303'.

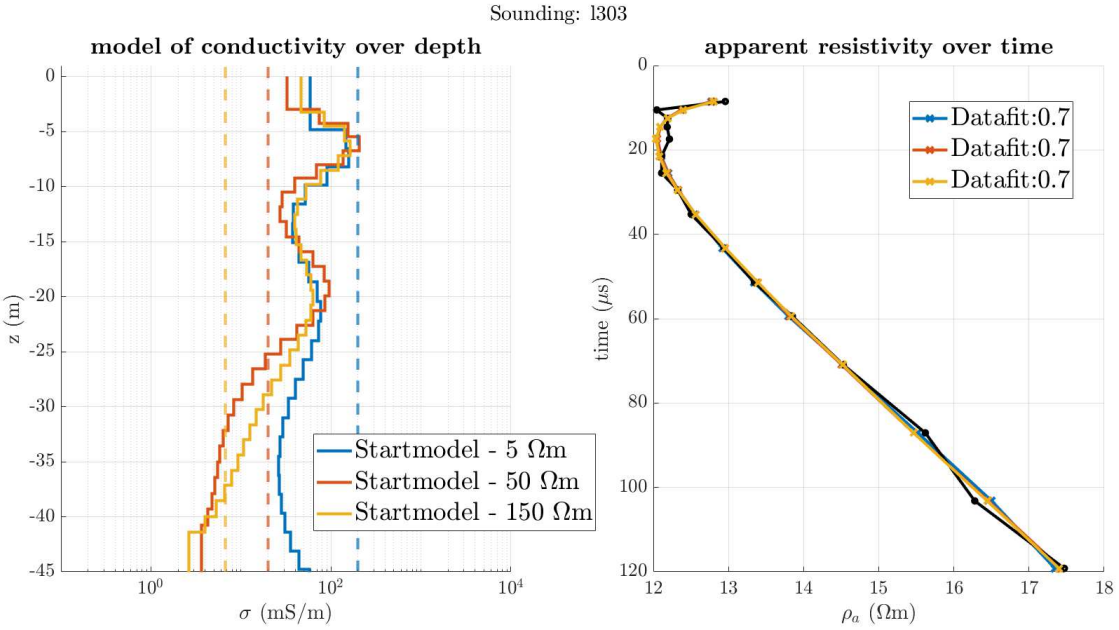

Figure 4.29: Inversion results using three different homogeneous start models with three different resistivity values. Exemplary for TEM sounding 'L303'. Left side: inversion models. Right side: data points used for inversion and the corresponding datafit for the three start models.

The three models look similar until a depth of approximately 40 m. At this depth the final model changes the direction depending on the resistivity value used in the start model. Consequently, the inversion model may be sensitive until a maximum depth of about 40 m. This value corresponds with the depth gained from the rule of thumb (35 m) for estimating the depth of investigation for a TEM loop (from Bücker et al. (2017)). A strong difference can be seen in the shallow depths in all three models. There the three models show bigger inconsistencies than in the regions below. This may be traced back to the filtering step prior to the inversion. In this step data was cut due to a low SNR. Later on, more datapoints were deleted in the early times to obtain a good fit. This deletion led to worse resolution in low depths.

ERT data was used to validate the resulting TEM inversion model.
The processing and inversion of the ERT data was done, as described in section 3.3.4, by Lukas Aigner to limit the scope of this thesis. Visualization was done by using MATLAB after choosing the best parameter combination of the ERT inversion results.
Different parameter values than those described in section 3.3.4 were used to obtain the

final inversion model:

- $err_{abs} = 0.001\ \Omega m$
- $err_{rel} = 10\ \%$
- $\lambda = 500$
- $z_{weight} = 0.005$

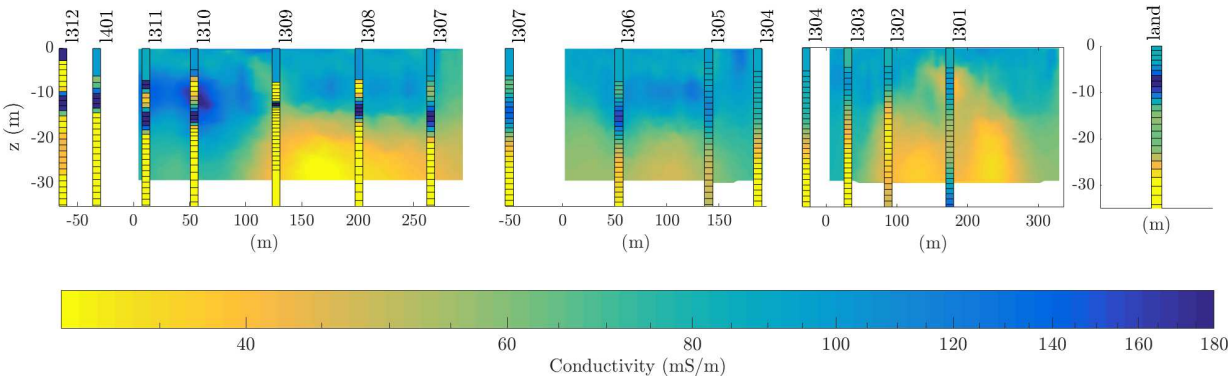

Figure 4.30: Comparison of TEM logs (in the front) and interpolation of ERT inversion data (in the back) from TEM soundings from Profile 3 including sounding 'L401' and 'land' and ERT Profiles 2, 10 and 11.

Figure 4.30 shows an overlay of ERT inversion data and TEM logs projected onto the ERT profiles. See 4.21 to get an idea of the positions of the ERT and TEM data shown below.

The subplot on the right shows the inversion result for the TEM sounding 'land' onshore. This sounding was collected after the waterborne measurements to get a comparison of measurements on land and on water. The resulting models off and on shore look similar, which means that the results are plausible.
The comparison of TEM and ERT match with one exception. In Figure 4.30 at the start of the left profile, from 0 to approximately 100 m (TEM: L312-L307 / ERT: profile 2) a strong difference between TEM and ERT is noticeable. TEM and ERT do not match well in this area. TEM either has a higher vertical resolution showing less conductive areas at shallow depths or with ERT the current only flows in the water and does not propagate more deeply. Therefore, a point (L401) from another TEM line was selected to compare to check if there was a problem during the TEM measurement, such as coupling. When comparing L401 with the surrounding TEM soundings (in Figure 4.30) it can clearly be seen that the data from this area looks similar. This means that there was no problem

with the TEM measurements. An explanation for the difference in TEM and ERT data can be that the ERT cable was not in a straight line when we started the measurement (shown in Figure 4.31).

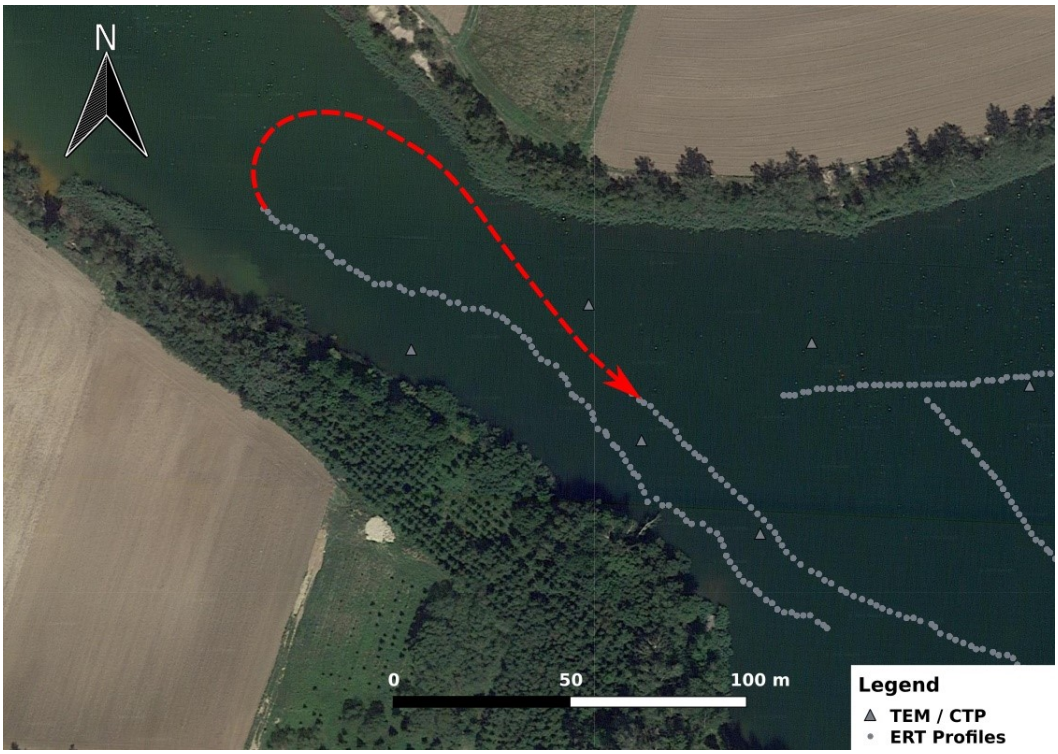

Figure 4.31: Approximated pathway of boat and ERT cable prior to measuring ERT profile 2. Possible reason for the difference in ERT and TEM data.

When the ERT cable forms a curve, the electrode spacing is smaller than expected. This may cause a lower penetration depth. This is a known problem for 2D inversions, when the electrodes are not in a straight line. A 3D inversion would be the better option but this would require known positions of the electrodes.

Coverage (or sensitivity) of the ERT measurements are examined in the following to get an idea of how deep the current propagated down into the water and the underlying structures. The coverage indicates how much the resulting model corresponds to the input data. In Figure 4.32 the coverage is plotted over depth for the three ERT profiles (2, 10 and 11).

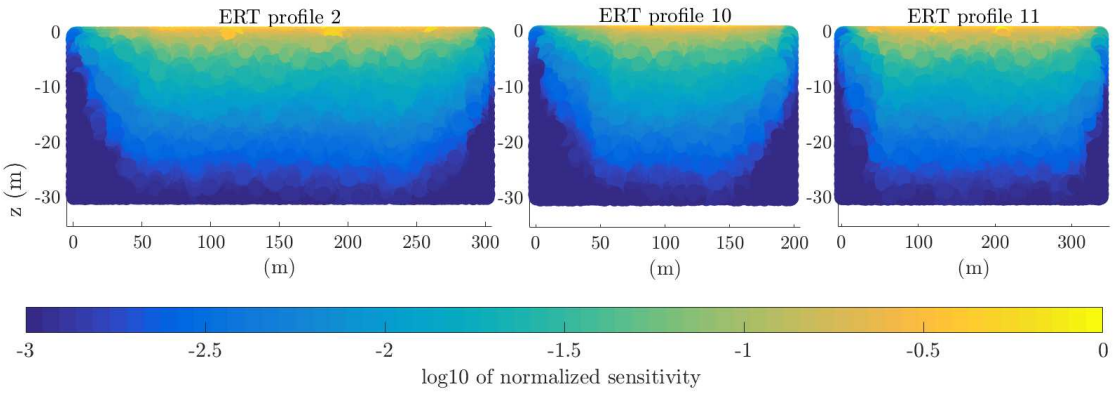

Figure 4.32: ERT coverage for profiles 2, 10 and 11.

The sensitivity shown in Figure 4.32 is normalized to the highest value and displayed as a decadic logarithm. Connecting the statement from above and the content from Figure 4.32, one can derive that at a depth of about 5 m only 10% of the sensitivity was left, meaning that most of the current during the ERT measurements was flowing in the water and did not propagate down into the lake bed.

To conclude this case study, it can be said that it is possible to delimit the sedimentary layer of a lake with TEM. However, as mentioned within the other two case studies, complementary geophysical data plays a crucial role with the processing/inversion and validation of the TEM results. Namely CTD data can be used as a-priori information for the inversion procedure. It can also help create a more realistic start model. As TEM data shows good agreement with the ERT data in most areas of the lake, it is likely that the resulting inversion model can be trusted.
For future off shore ERT measuring campaigns it should be ensured that the cable forms a straight line at the start of an ERT profile or the positions of the electrodes should be known to avoid a similar error as described above.
According to the resulting inversion model, the sediment layer is thicker where the lake is deeper and, correspondingly the layer is thinner where the lake is more shallow.

5 Conclusion

The aim of this thesis was to determine whether TEM is capable of delineating the sedimentary layer underneath lakes and to detect stratification in the lake water.
A floatable carrier structure had to be built to be able to conduct waterborne TEM measurements. The construction was built on the basis of different previous studies.
Three case studies were carried out to verify the hypothesis presented.

In the first case study (at Laacher See) it was not possible to detect the stratification of the lake water. Due to unforeseen disturbances the data was erroneous. ERT measurements, which were conducted for an improved interpretation, were also affected by errors. First proposed solutions would be to use a non-metallic boat with the TEM equipment and to attach buoys or similar floating structures onto the ERT water cable. The only statement that can be made is that the known stratification in summer can be seen in the ERT data from August 2020.
Within the second case study, data from a field campaign in Mexico was processed. The aim was to delineate the sedimentary layer underneath the water column, using TEM. No complementary data was available to validate the inversion results. Therefore, several inversion approaches were compared. This should be taken into account when dealing with the results. A sedimentary layer can be determined in some parts of the lake examined but further investigations would be necessary to completely ensure the correctness of the results.
The third case study (at Langau) aimed at finding the sedimentary layer underneath the lake while also using a CTD probe and waterborne ERT measurements. The advantages of complementary methods were presented and the consistent results show a layer that might resolve the sediments on the lake floor. While reviewing the data it became clear that there were problems at the beginning of the examined ERT profile. The problems probably arose because the water cable did not form a straight line, which shortened the distance between the electrodes. Therefore, before starting the ERT measurement, it should be ensured that the cable is in a straight line.

The results from the different case studies show that it is possible to delimit the sedimentary layer with TEM. However, it is strongly recommended to use a multi-methodical approach to help with the interpretation of TEM data. Furthermore, an interdisciplinary approach would be helpful to validate the obtained results.

References

- AESCHBACH-HERTIG, W., et al. *Quantification of gas fluxes from the subcontinental mantle: The example of Laacher See, a maar lake in Germany.* Geochimica et cosmochimica acta, 1996, 60. Jg., Nr. 1, S. 31-41.
- AESCHBACH-HERTIG, W., et al. *Accumulation of mantle gases in a permanently stratified volcanic Lake (Lac Pavin, France).* Geochimica et Cosmochimica Acta, 1999, 63. Jg., Nr. 19-20, S. 3357-3372.
- AIGNER, Lukas. *Improving the Understanding of Transient Electromagnetic Signals for Near-surface Applications by Assessing the Turn-off Ramp.* Wien, 2019. Print.
- Applied Electromagnetic Research (AEMR), 2018. *TEM-FAST 48 – Manual, Version 8a*, the Netherlands.
- ARCHIE, Gustave E., et al. *The electrical resistivity log as an aid in determining some reservoir characteristics.* Transactions of the AIME, 1942, 146. Jg., Nr. 01, S. 54-62.
- BARRETT, Brian, et al. *River sediment salt-load detection using a water-borne transient electromagnetic system.* Journal of Applied Geophysics, 2005, 58. Jg., Nr. 1, S. 29-44.
- BARSUKOV, Pavel O.; FAINBERG, Edward B.; KHABENSKY, Eugene O. *Shallow investigations by TEM-FAST technique: Methodology and examples.* In: Electromagnetic sounding of the Earth's interior. Elsevier, 2015. S. 47-78.
- BINLEY, Andrew; KEMNA, Andreas. *DC resistivity and induced polarization methods.* In: Hydrogeophysics. Springer, Dordrecht, 2005. S. 129-156.
- BÜCKER, Matthias, et al. *Geoelectrical and electromagnetic methods applied to paleolimnological studies: Two examples from desiccated lakes in the Basin of Mexico.* Boletín de la Sociedad Geológica Mexicana, 2017, 69. Jg., Nr. 2, S. 279-298.
- BÜCKER, Matthias & FLORES OROZCO, Adrián & GALLISTL, Jakob & STEINER, Matthias & AIGNER, Lukas & HOPPENBROCK, Johannes & GLEBE, Ruth & BARRERA, Wendy & PAZ, Carlos & PÉREZ, José & BUCKEL, Johannes & HÖRDT, Andreas & SCHWALB, Antje & PÉREZ, Liseth. (2020). *Water-and land-borne geophysical surveys before and after the sudden water-level decrease of two large karst lakes in southern Mexico.* 10.5194/se-2020-75.

- BUTLER, Karl E. *Trends in waterborne electrical and EM induction methods for high resolution sub-bottom imaging.* Near Surface Geophysics, 2009, 7. Jg., Nr. 4, S. 241-246.
- CHRISTIANSEN, Anders Vest; AUKEN, Esben; SØRENSEN, Kurt. *The transient electromagnetic method.* In: Groundwater geophysics. Springer, Berlin, Heidelberg, 2006. S. 179-225.
- EVERETT, Mark E. *Near-surface applied geophysics.* Cambridge University Press, 2013.
- GOLDMAN, M.; NEUBAUER, F. M. *Groundwater exploration using integrated geophysical techniques.* Surveys in geophysics, 1994, 15. Jg., Nr. 3, S. 331-361.
- GOLDMAN, Mark; GVIRTZMAN, Haim; HURWITZ, Shaul. *Mapping saline groundwater beneath the Sea of Galilee and its vicinity using time domain electromagnetic (TDEM) geophysical technique.* Israel Journal of Earth Sciences, 2004, 53. Jg., Nr. 3-4, S. 187-197.
- GONÇALVES, Rui Manuel Domingos. *Hydrochemical water prediction (water quality) with transient electromagnetic soundings (TEM).* 2012. Doktorarbeit. Universidade de Lisboa (Portugal).
- GONZALEZ-ALVAREZ, Ignacio & ANAND, RR & HOUGH, Robert & SALAMA, Walid & LAUKAMP, Carsten & SWEETAPPLE, Marcus & LEY-COOPER, Alan & SONNTAG, I & LINTERN, Melvyn & IBRAHIMI, Tania & LEGRAS, Monica & WALSHE, John. (2014). *Greenfields geochemical exploration in a regolith dominated terrain: the Albany-Fraser Orogen/Yilgarn Craton margin.* 10.13140/2.1.1051.9362.
- GÜNTHER, Thomas; RÜCKER, Carsten. *Boundless Electrical Resistivity Tomography BERT 2–the user tutorial.* 2015.
- HANSON, B. R.; KAITA, K. R*esponse of electromagnetic conductivity meter to soil salinity and soil-water content.* Journal of irrigation and Drainage Engineering, 1997, 123. Jg., Nr. 2, S. 141-143.
- HATCH, Michael; MUNDAY, Tim; HEINSON, Graham. *A comparative study of in-river geophysical techniques to define variations in riverbed salt load and aid managing river salinization.* Geophysics, 2010, 75. Jg., Nr. 4, S. WA135-WA147.

- HUNTLEY, David; BOBROWSKY, Peter; BEST, Melvyn. *Combining terrestrial and waterborne geophysical surveys to investigate the internal composition and structure of a very slow-moving landslide near Ashcroft, British Columbia, Canada.* In: Workshop on World Landslide Forum. Springer, Cham, 2017. S. 179-190.
- In-Situ, *Operator's Manual - Aqua TROLL 100 & 200 Sonde*, 0061340 | | 08/2016.
- KAMINSKY Alex - Zond software corporation. (2001). *ZondTEM1d.* `http://zond-geo.com/english/zond-software/electromagnetic-sounding/zondtem1d/`
- KATZNELSON, Revital. *DQM Information Paper 3.1. 3 Conductivity/Salinity Measurement Principles and Methods.*
- KEAREY, Philip; BROOKS, Michael; HILL, Ian. *An introduction to geophysical exploration.* John Wiley & Sons, 2013.
- KNÖDEL, Klaus; KRUMMEL, Heinrich; LANGE, Gerhard (Hg.). *Handbuch zur Erkundung des Untergrundes von Deponien und Altlasten.* Springer Science & Business Media, 2005.
- MARCHANT, David. *Induced polarization effects in inductive source electromagnetic data.* 2015. Doktorarbeit. University of British Columbia.
- MCNEILL, J. D. *Principles and application of time domain electromagnetic techniques for resistivity sounding.* Geonics, 1994.
- MENKE, William. *Describing inverse problems.* 2012.
- MOLLIDOR, L., et al. *Float-transient electromagnetic method: in-loop transient electromagnetic measurements on Lake Holzmaar, Germany.* Geophysical Prospecting, 2013, 61. Jg., Nr. 5, S. 1056-1064.
- NABIGHIAN, Misac N., et al. *Time domain electromagnetic prospecting methods.* Electromagnetic methods in applied geophysics, 1991, 2. Jg., Nr. part A, S. 427-509.
- ØYBEKK, Vilde Jørdre. *Application of waterborne electrical resistivity tomography and ground penetrating radar in the delta area of Numedalslågen, Norway.* 2018. Masterarbeit. Norwegian University of Life Sciences, Ås.
- RAICHE, A. P. *The effect of ramp function turn-off on the TEM response of layered earth.* Exploration Geophysics, 1984, 15. Jg., Nr. 1, S. 37-41.

- REID. J. (2014). *Introduction to Geophysical Modelling and Inversion.* Geophysical inversion for mineral exploration. September 2, City West Function Centre, West Perth, WA

- REYNOLDS, John M. *An introduction to applied and environmental geophysics.* John Wiley & Sons, 2011.

- RHOADES, J. D. *Salinity: Electrical conductivity and total dissolved solids.* Methods of Soil Analysis: Part 3 Chemical Methods, 1996, 5. Jg., S. 417-435.

- RUCKER, Dale F.; NOONAN, Gillian E.; GREENWOOD, William J. *Electrical resistivity in support of geological mapping along the Panama Canal.* Engineering Geology, 2011, 117. Jg., Nr. 1-2, S. 121-133.

- RÜCKER, C., GÜNTHER, T., WAGNER, F.M., 2017. *pyGIMLi: An open-source library for modelling and inversion in geophysics*, Computers and Geosciences, 109, 106-123, doi: 10.1016/j.cageo.2017.07.011.

- TEAM, Clean Water. *Electrical conductivity/salinity fact sheet*, FS-3.1. 3.0 (EC). The Clean Water Team Guidance Compendium for Watershed Monitoring and Assessment, Version, 2004, 2. Jg.

- SPIES, Brian R. *Depth of investigation in electromagnetic sounding methods.* Geophysics, 1989, 54. Jg., Nr. 7, S. 872-888.

- TELFER, Andrew L., et al. *Instream nanoTEM: Providing increased resolution to stream salinisation and floodplain processes along the river Murray, southeast Australia.* Australasian Journal of Water Resources, 2005, 9. Jg., Nr. 2, S. 155-161.

- TELFORD, William Murray, et al. *Applied geophysics.* Cambridge university press, 1990.

- YOGESHWAR, Pritam. *A resistivity-depth model of the central Azraq basin area, Jordan: 2D forward and inverse modeling of time domain electromagnetic data.* 2014. Doktorarbeit. Universitäts-und Stadtbibliothek Köln.

- YOGESHWAR, Pritam, et al. *Innovative boat-towed transient electromagnetics — Investigation of the Furnas volcanic lake hydrothermal system, Azores.* Geophysics, 2020, 85. Jg., Nr. 2, S. E41-E56.

Appendix

For additional figures on the three case studies visit
`https://owncloud.tuwien.ac.at/index.php/s/V4d0UkgcmV3FTZN?path.....=%2FAbgabe_Diplomarbeit_Hoegenauer%2FAppendix_Hoegenauer`.
This link is time limited.
If the time limit is reached, please contact Associate Prof. Dr.rer.nat. Adrian Flores-Orozco (*adrian.flores-orozco@tuwien.ac.at*).